Egyptian Journal of Geology, v. 63, 2019, p.215-236

PETROLOGY AND GEOCHEMISTRY OF WADI ATALLA EL-MURR METABASALTS, EASTERN DESERT, EGYPT: VOLCANISM IN A MATURE NEOPROTEROZOIC BACK-ARC BASIN

Ayman E. Maurice

Geology Department, Faculty of Science, Helwan University, 1795 Cairo, Egypt

ABSTRACT

The mafic volcanic rocks of Wadi Atalla El-Murr, Eastern Desert, Egypt, comprise aphyric and porphyritic metabasalts composed of variably altered pyroxene and plagioclase. In the porphyritic metabasalts, the phenocrysts are dominated by augite either as individual crystals or as aggregates forming glomeroporphyritic texture. The plagioclases encompass a wide compositional range from labradorite (An = ~73%) to albite (An = 0.61%), reflecting seafloor hydrothermal alteration and metamorphism. The composition of the augite indicates crystallization from a subalkaline magma, overlapping the chemical characteristics of pyroxenes from island arc and ocean-floor basalts. The whole-rock compositions of representative samples reveal that these basalts are characterized by low K_2O contents (<1 wt%) and have tholeiitic affinity. The chondrite-normalized REE patterns of the metabasalts display slight enrichment in LREE relative to HREE (La/Yb_n = 1.08-1.70) and their MORB-normalized spider diagrams show variable LILE enrichment, variable depletion in most HFSE and a small negative Nb anomaly, suggesting derivation from a mantle source modified by a subduction component. However, these tholeiitic basalts differ in their geochemical features from Neoproterozoic nascent intra-oceanic island arc tholeiites (IAT), and mostly occupy the MORB or BABB field on conventional tectonomagmatic discrimination diagrams. The mixed MORB/IAT geochemical characteristics of the Wadi Atalla El-Murr basalts most closely resemble those of basalts generated in modern back-arc environments affected by minor subduction input, implying eruption during the earliest mature stage of a Neoproterozoic back-arc basin. The present and published data of the metavolcanic rocks of Egyptian ophiolites revealed that they comprise BABB and MORB compositions. The majority of ophiolite metavolcanics of Egypt formed in subduction-related settings, from mantle sources slightly to significantly modified by input of a subduction component, implying generation at different stages of development of Neoproterozoic supra-subduction zone systems.

Keywords: Neoproterozoic ophiolites, Ophiolite settings, Back-arc basins, BABB, Eastern Desert

INTRODUCTION

Oceanic crust has been essentially created along mid-oceanic ridges or smaller back-arc spreading centers (Wilson, 1989), however, the erupted volcanics in these settings may differ geochemically. Volcanic rocks erupted along modern back-arcs, such as Lau basin (e.g. Pearce et al., 1995; Keller et al., 2008; Tian et al., 2011), Okinawa Trough (e.g. Shinjo et al., 1999), Japan Sea back-arc basin (e.g. Hirahara et al., 2015), Manus back-arc basin (Sinton et al., 2003), Mariana Trough (e.g. Gribble et al., 1998; Pearce et al., 2005) and East Scotia Sea (e.g. Tarney et al., 1981; Fretzdorff et al., 2002), show geochemical variations from typical MORB to typical arc volcanics (e.g. Fretzdorff et al., 2002; Pearce et al., 1995; Keller et al., 2008). The variable arc signature in back-arc lavas is related to the proximity of spreading center from volcanic arc (e.g. Tarney et al., 1981; Pearce et al., 1995) and to the amount and type (fluid or melt) of subduction component (e.g. Pearce et al., 1995; Hirahara et al., 2015). Although back-arc lavas are essentially basaltic in composition, some back-arc basins erupts more evolved volcanics (e.g. Vallier et al., 1991; Pearce et al., 1995; Tian et al., 2011).

Neoproterozoic intra-oceanic volcanics of the Eastern Desert of Egypt comprise ophiolite (e.g. Abd El-Rahman et al., 2009a&b; Basta et al., 2011) and island arc (e.g. Maurice et al., 2012) metavolcanics. The ophiolite metavolcanics are essentially basalts, basaltic andesites and andesites with tholeiitic to

transitional character (e.g. Abd El-Rahman et al., 2009a; Basta et al., 2011) whereas the island arc metavolcanics range from tholeiitic basalts (e.g. Maurice et al., 2012) to calc-alkaline andesites (e.g. Stern et al., 1981). Although the ophiolite and island arc metavolcanics are termed, respectively, older and younger metavolcanics (Stern et al., 1981), U-Pb zircon dating of these volcanics revealed that they have similar ages (~750 Ma, Ali et al., 2009). The ophiolite metavolcanics are considered to be generated in a major ocean basin (e.g. Zimmer et al., 1995), back-arc (e.g. El-Sayed et al., 1999; Abd El-Rahman et al., 2009a; Basta et al., 2011) or incipient fore-arc (Abd El-Rahman et al., 2009b). On the other hand, the arc tholeiitic basalts and calc-alkaline andesites were formed during nascent (Maurice et al., 2012) and mature stages (Stern et al., 1981), respectively, of intra-oceanic island arcs. Recently, Abdel-Karim et al. (2019) proposed that the tholeiitic/calc-alkaline Shadli bimodal metavolcanics were erupted in arc setting. The third class of the Neoproterozoic volcanic rocks in the Eastern Desert of Egypt is represented essentially by calc-alkaline andesitic/dacitic Dokhan volcanics (e.g. Basta et al., 1980; Ressetar and Monrad; 1983; Abdel-Rahman, 1996; Moghazi, 2003; Eliwa et al., 2006). The tectonic setting and the origin of the Dokhan volcanics have been controversial (Maurice et al., 2018 and references therein).

This study present petrography, mineral chemistry and whole-rock geochemistry of Neoproterozoic metabasalts from Wadi Atalla El-Murr area, Central Eastern Desert, Egypt, aiming to decipher their tectonic setting. The nature of the Neoproterozoic mantle source of the parental magmas of these oceanic basalts and the subduction component contributed to their genesis have been evaluated. The implication of the results of the present study for classification of Eastern Desert ophiolite metavolcanics has been considered.

GEOLOGIC SETTING

The Wadi Atalla El-Murr area is part of Wadi Atalla district, Central Eastern Desert, Egypt. This area hosts two gold occurrences, namely Atalla El-Murr and El-Nabsh El-Kidim. The mapped area (Fig. 1) is covered by serpentinites, volcanic rocks, felsites, younger gabbros and younger granites (Essawy and Abu Zeid, 1972; Ghoneim, 1973; Wassef et al., 1973; Bakhit, 1994; Basta et al., 1996). The small sepentinites mass in the southwestern part of the mapped area constitutes part of mountainous ultramafic chain which extends NW-ward from Fawakhir area in the south. The volcanic rocks cover most of the study area and crop out essentially in the eastern side of Wadi Atalla. They were previously mapped as island arc volcanics (Bakhit, 1994; Basta et al., 1996), and comprise mafic and felsic varieties. The mafic volcanics are the dominant rocks, occupying most of the study area, while the felsic volcanics are exposed in the southeastern part. The gold occurrences are located within the mafic volcanics mass, which is dissected by numerous quartz veins. Taman (1996) studied volcanic rocks in part of Wadi Atalla El-Murr area and proposed that they comprise rhyolitic flows and tuffs which are cut by intermediate and mafic dykes, quartz veins and rare jasperoid veins. In the western part of the study area, the felsites are exposed as NW-trending rugged belt intruding the metavolcanics (Ghoneim, 1973; Bakhit, 1994; Basta et al., 1996). The younger gabbros were recorded by Bakhit (1994) as cone hills in the southern part of the study area. The younger granites are represented by a small pluton traversed by Wadi Atalla El-Murr in the northern part of the study area. They are intruding the metavolcanics and cut by dykes.

PETROGRAPHY

The metabasalts of Wadi Atalla El-Murr area are classified petrographically into non-porphyritic basalt, vitrophyre and porphyritic basalt, which is occasionally amygdaloidal. The variation of texture from very fine-grained through vitrophyre to porphyritic reflects variable degrees of cooling from quenching to slower rate of cooling. The opaque minerals are represented essentially by ilmenite which is mostly altered to titanite.

Non-porphyritic basalt

The rock is very fine- to fine-grained, composed of fine pyroxene and very fine to fine plagioclase laths (Fig. 2A). Sometimes, pyroxene is present as rare microphenocrysts. The pyroxenes are commonly altered to tremolite and chlorite. Carbonate and chlorite are secondary minerals. The rock is occasionally dissected by carbonates-quartz and quartz veinlets.

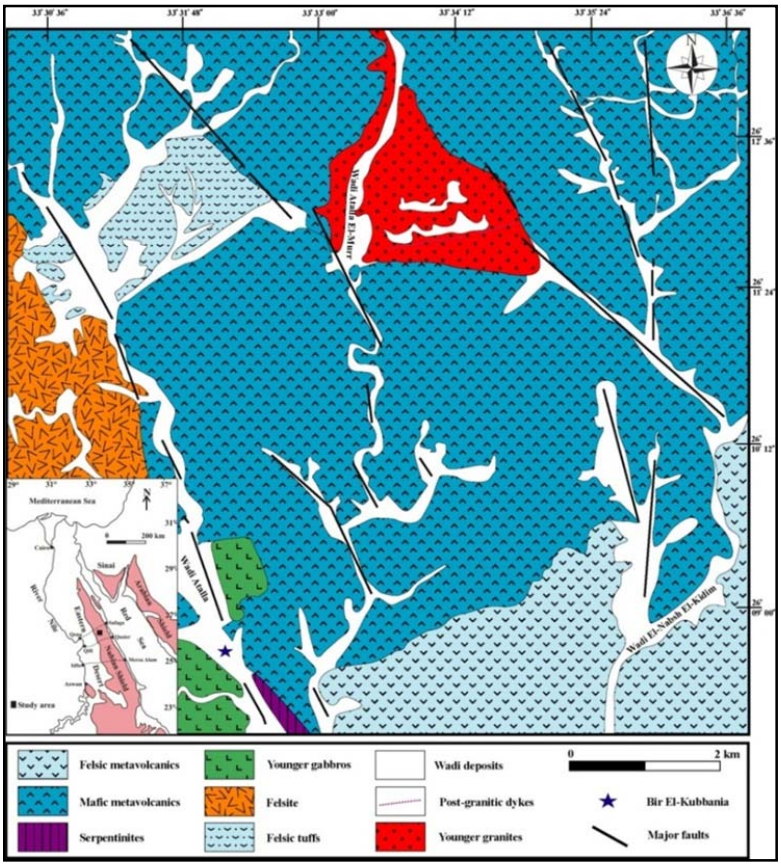

Fig. 1: Location and geologic map of Wadi Atalla El-Murr area (modified after Wassef et al., 1973), Central Eastern Desert (CED), Egypt.

Vitrophyre

The rock is composed of pyroxene phenocrysts/microphenocrysts and plagioclase microphenocrysts within very fine-grained groundmass (Fig. 2B). The phenocrysts are mostly pyroxene, while the plagioclase microphenocrysts are subordinate and occur as thin prisms and laths. The very fine-grained groundmass is composed of devitrified glassy material. The pyroxene is partly altered to chlorite and plagioclase is slightly sericitized. The rock is dissected with chlorite and chlorite-quartz veins.

Porphyritic basalt

The rock is composed of pyroxene phenocrysts and occasionally rare plagioclase phenocrysts in fine-grained groundmass (Fig. 2C). Pyroxene phenocrysts occur either as equant individual crystals or as clusters, forming glomeroporphyritic texture (Fig. 2D). Pyroxene is also present as finer prismatic crystals. The pyroxene is partly altered to tremolite and chlorite (Fig. 2E), and plagioclase is variably sericitized. The rock is sometimes amygdaloidal and displays quench texture (Fig. 2F). The amygdales are irregular in shape and filled with chlorite and/or calcite. The fine-grained groundmass is composed of fine prismatic pyroxene and plagioclase as well as devitrified glass. The rock is dissected by veinlets of chlorite, chlorite-epidote and carbonate with or without chlorite.

ANALYTICAL TECHNIQUES

Representative whole-rock samples of the different basalts were analyzed for major, trace and rare earth elements using wave-length dispersive X-ray fluorescence spectrometer (WD-XRF, Axios, PANalytical) and laser ablation - inductively coupled plasma - mass spectrometry (LA-ICP-MS). Pyroxene and plagioclase analyses were carried out using a JEOL JXA-8200 electron probe microanalyzer equipped with five wavelength dispersive spectrometers (WDS). The bulk-rock and electron microprobe analyses were performed at the Institute of Geochemistry and Petrology, ETH-Zürich, Switzerland. The description and detection limits of the methods used in whole-rock and minerals analyses are similar to those given in Basta et al. (2011, 2017).

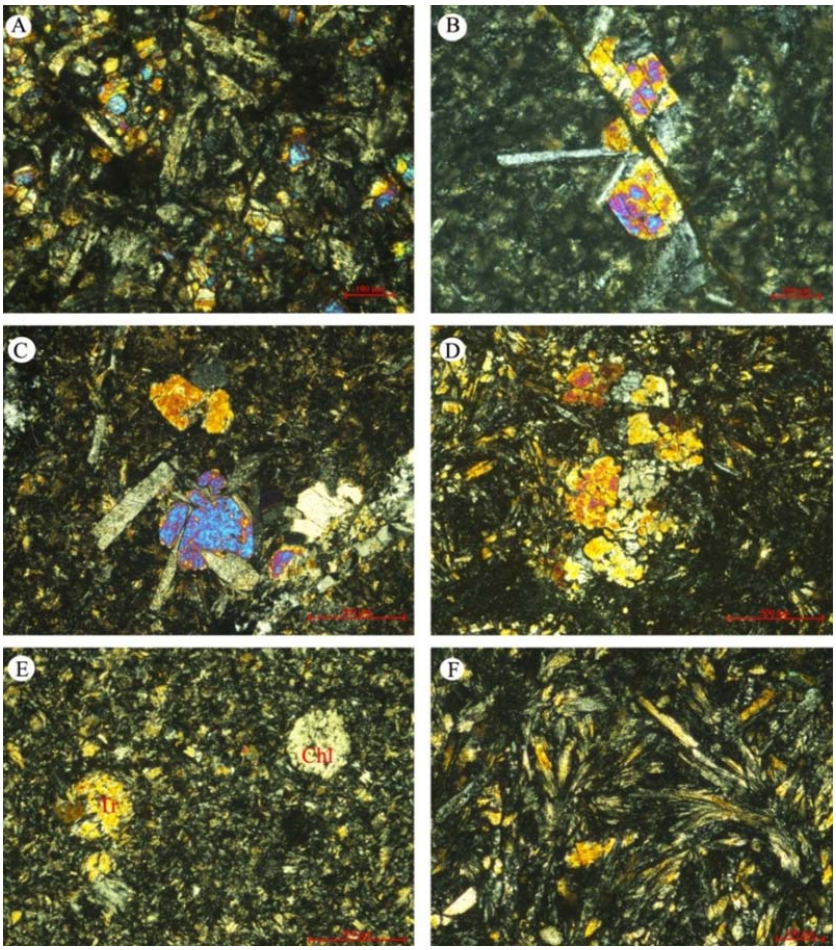

Fig. 2: Petrographic characteristics of Wadi Atalla El-Murr metabasalts. (A) Aphyric metabasalt composed of pyroxene and plagioclase, (B) Vitrophyre showing pyroxene phenocrysts and plagioclase microphenocrysts in devitrified groundmass, (C) Porphyritic basalt showing pyroxene and plagioclase phenocrysts/microphenocrysts, (D) Porphyritic basalt showing glomeroporphyritic texture, (E) Porphyritic basalt showing pyroxene phenocrysts altered to tremolite (Tr) and chlorite (Chl), (F) Quench texture in porphyritic basalt, reflecting rapid cooling. All photos are in crossed nicols.

MINERAL CHEMISTRY

Fresh relics of pyroxene and plagioclase of Wadi Atalla El-Murr metabasalts were analyzed by electron microprobe. The composition and structural formula of the analyzed pyroxene and plagioclase are given in Tables 1 and 2.

Pyroxene

The pyroxenes of Wadi Atalla El-Murr metabasalts belong to the calcic pyroxenes with CaO contents ranging from 15-21 wt% (average = 19 wt%) and are classified as augites (Fig. 3A) following the pyroxene classification of Morimoto et al. (1988). The Al_2O_3 contents vary from 1.43-3.60 wt% (average = 2.31 wt%). These pyroxenes are characterized by low TiO_2 (0.25-0.75 wt%, average = 0.40 wt%) and Cr_2O_3 (0-0.48 wt%, average = 0.14 wt%) contents and are similar to pyroxenes crystallize from subalkaline magmas (Fig. 3B). They have mineral chemical characteristics akin to those of pyroxenes of both island arc and ocean-floor basalts (Fig. 3C and D).

Plagioclase

The analyzed plagioclases of Wadi Atalla El-Murr metabasalts show wide range of CaO (0.11-14.45 wt%, average = 5.53 wt%) and Na_2O (2.90-9.89 wt%, average = 7.27 wt%) contents. They cover wide

compositional range from labradorite to albite (Table 2). The high An contents (up to ~73%) of plagioclases indicate primary composition, whereas the low An content (down to 0.61%) of some plagioclases reflects post-magmatic modifications. Such broad variation in the chemical composition of plagioclases and presence of albite in these basalts can be attributed to sea-floor hydrothermal alteration and metamorphism.

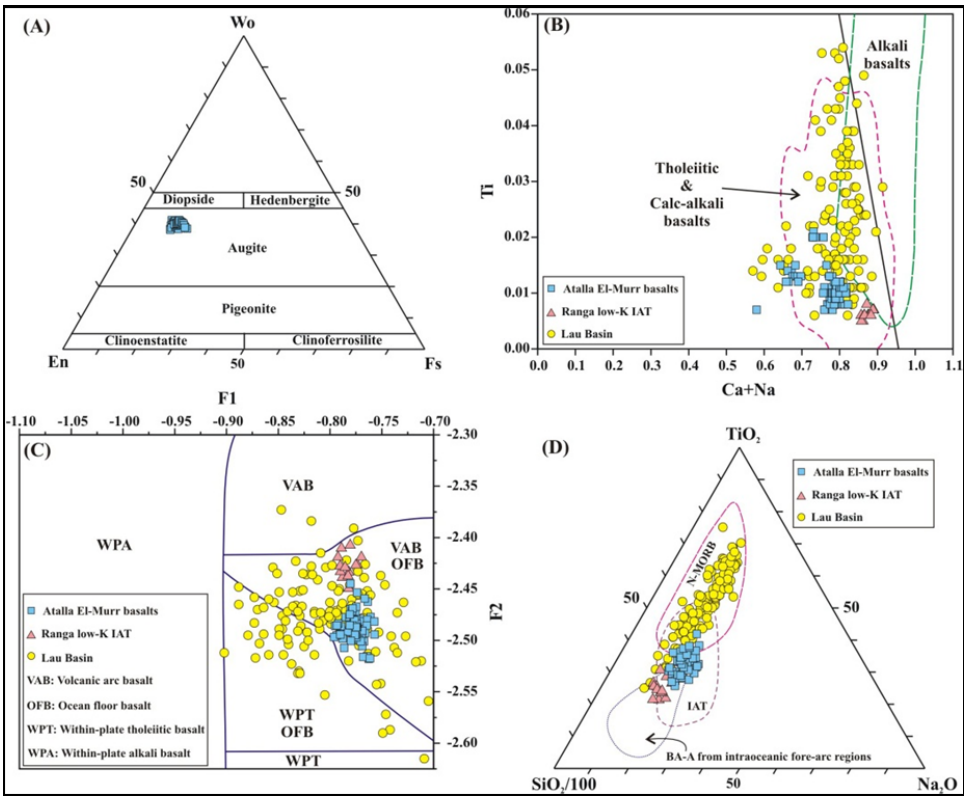

Fig. 3: Compositional features of the pyroxene of Wadi Atalla El-Murr basalts. (A) En-Fs-Wo diagram for nomenclature of pyroxene (after Morimoto et al., 1988), (B) Ti vs Ca+Na diagram (after Leterrier et al., 1982) for evaluation of magma type, (C) F1-F2 diagram (after Nisbet and Pearce, 1977) and (D) TiO_2-Na_2O-SiO_2/100 diagram (after Beccaluva et al., 1989) for tectonic setting discrimination. Data sources: pyroxene composition of Lau Basin back-arc basalts after Hawkins and Allan (1994); pyroxene composition of Neoproterozoic IAT of Wadi Ranga (South Eastern Desert) after Maurice et al. (2012).

GEOCHEMISTRY

Thirteen representative samples of Wadi Atalla El-Murr mafic volcanic rocks have been selected for major, trace and rare earth elements analyses using XRF and LA-ICP-MS techniques. The compositions of the analyzed whole-rock samples are given in Table 3.

The mafic volcanic rocks of Wadi Atalla El-Murr are classified as basalt (Fig. 4A). Moreover, the basalts plot in the field of the older metavolcanics (OMV) of Eastern Desert (Fig. 4A). The LOI values of all analyzed metabasalts (except one) are less than or equal to 4 wt% indicating that the magmatic composition of these rocks was not significantly modified by alteration and metamorphism (Polat et al., 2002). The metabasalts have low K_2O contents (0.15-0.94 wt%) similar to oceanic volcanic rocks derived from depleted mantle source (Maurice et al., 2012). The MgO contents of the metabasalts range from 6.4-9.6 wt% and Mg# [(MgO/(MgO+FeO*)] varies from 52.7 to 64.8, suggesting that some of these samples do not represent primitive melts. The metabasalts are similar to subalkaline mafic volcanic rocks (Fig. 4A), and have tholeiitic nature (Fig. 4B).

Table 1. Composition and structural formula of pyroxene of Wadi Atalla El-Murr metabasalts, Central Eastern Desert, Egypt.

Sample	E3	E3	E3	E3	E3	E3	E3	E3	E3	E3	E3	E3	E3	E3	E3	E3	E3	E3	E3	E3	E3
No.	1	2	3	4	5	6	7	8	9	10	11	12	13	14	15	16	17	18	19	20	21
SiO_2	52.47	52.46	53.03	53.08	52.98	53.40	52.93	53.61	53.00	54.10	53.00	53.29	53.33	52.92	53.40	52.20	52.28	52.06	52.37	52.26	53.45
TiO_2	0.49	0.35	0.30	0.31	0.30	0.30	0.29	0.27	0.32	0.27	0.31	0.29	0.31	0.34	0.32	0.37	0.37	0.37	0.36	0.41	0.25
Al_2O_3	2.90	2.92	2.29	2.25	2.34	2.14	2.11	1.98	2.71	1.43	2.33	2.16	2.37	2.60	2.27	3.38	3.32	3.47	3.25	3.56	1.91
FeO	8.14	6.45	5.99	5.94	6.11	6.02	5.90	6.50	6.24	8.96	6.41	6.39	6.68	6.32	6.54	6.42	6.58	6.53	6.49	6.62	6.26
MnO	0.21	0.17	0.15	0.14	0.16	0.14	0.16	0.18	0.16	0.28	0.17	0.17	0.19	0.16	0.20	0.17	0.18	0.17	0.18	0.18	0.18
MgO	18.48	17.47	17.47	17.63	17.58	17.62	17.69	18.42	17.51	20.57	17.94	18.01	18.29	17.76	18.29	17.18	17.06	17.47	17.12	17.28	18.06
CaO	16.80	19.93	20.38	20.46	20.29	20.58	20.69	19.27	20.16	14.74	19.64	19.84	19.51	19.56	19.70	20.26	19.89	19.51	19.99	19.79	19.66
K_2O	0.00	0.00	0.00	0.00	0.00	0.00	0.01	0.00	0.00	0.01	0.01	0.00	0.00	0.00	0.00	0.01	0.00	0.00	0.01	0.00	0.01
Na_2O	0.19	0.23	0.15	0.20	0.19	0.17	0.21	0.19	0.20	0.12	0.19	0.21	0.17	0.24	0.16	0.24	0.24	0.24	0.26	0.23	0.19
Cr_2O_3	0.06	0.24	0.30	0.25	0.29	0.28	0.25	0.17	0.25	0.06	0.21	0.16	0.14	0.18	0.15	0.22	0.18	0.36	0.33	0.29	0.18
Total	99.74	100.21	100.06	100.27	100.24	100.65	100.24	100.60	100.56	100.55	100.21	100.53	100.99	100.08	101.01	100.45	100.10	100.18	100.35	100.62	100.15
Formula based on 6 oxygens																					
Si	1.922	1.912	1.937	1.933	1.931	1.939	1.927	1.943	1.926	1.959	1.930	1.934	1.927	1.930	1.929	1.899	1.910	1.898	1.909	1.899	1.947
Ti	0.014	0.010	0.008	0.008	0.008	0.008	0.008	0.007	0.009	0.007	0.008	0.008	0.008	0.009	0.009	0.010	0.010	0.010	0.010	0.011	0.007
Al (T)	0.078	0.088	0.063	0.067	0.069	0.061	0.073	0.057	0.074	0.041	0.070	0.066	0.073	0.070	0.071	0.101	0.090	0.102	0.091	0.101	0.053
Al (M1)	0.047	0.038	0.036	0.029	0.032	0.030	0.018	0.028	0.042	0.020	0.031	0.027	0.028	0.041	0.025	0.044	0.053	0.047	0.048	0.051	0.029
Fe^{3+} (T)	0.000	0.000	0.000	0.000	0.000	0.000	0.000	0.000	0.000	0.000	0.000	0.000	0.000	0.000	0.000	0.000	0.000	0.000	0.000	0.000	0.000
Fe^{3+}(M1)	0.015	0.040	0.013	0.028	0.026	0.019	0.047	0.023	0.022	0.013	0.029	0.033	0.037	0.022	0.035	0.047	0.028	0.041	0.032	0.035	0.018
Fe^{2+}	0.234	0.156	0.170	0.153	0.161	0.164	0.132	0.175	0.168	0.258	0.166	0.161	0.165	0.171	0.162	0.148	0.173	0.158	0.166	0.166	0.173
Mn	0.007	0.005	0.005	0.004	0.005	0.004	0.005	0.006	0.005	0.009	0.005	0.005	0.006	0.005	0.006	0.005	0.006	0.005	0.005	0.005	0.006
Mg	1.009	0.949	0.951	0.957	0.955	0.954	0.960	0.995	0.948	1.110	0.974	0.975	0.985	0.965	0.985	0.932	0.929	0.949	0.930	0.936	0.981
Ca	0.659	0.778	0.798	0.798	0.792	0.801	0.807	0.748	0.785	0.572	0.766	0.772	0.755	0.764	0.762	0.790	0.779	0.762	0.781	0.770	0.767
K	0.000	0.000	0.000	0.000	0.000	0.000	0.000	0.000	0.000	0.000	0.001	0.000	0.000	0.000	0.000	0.001	0.000	0.000	0.000	0.000	0.000
Na	0.013	0.016	0.011	0.014	0.013	0.012	0.015	0.013	0.014	0.009	0.013	0.015	0.012	0.017	0.011	0.017	0.017	0.017	0.018	0.016	0.014
Cr	0.002	0.007	0.009	0.007	0.008	0.008	0.007	0.005	0.007	0.002	0.006	0.005	0.004	0.005	0.004	0.006	0.005	0.010	0.010	0.008	0.005
Total	4.000	4.000	4.000	4.000	4.000	4.000	4.000	4.000	4.000	4.000	4.000	4.000	4.000	4.000	4.000	4.000	4.000	4.000	4.000	4.000	4.000
En	52.44	49.20	49.12	49.32	49.27	49.12	49.19	51.14	49.20	56.59	50.18	50.10	50.57	50.09	50.49	48.48	48.54	49.56	48.60	48.93	50.44
Fs	13.30	10.46	9.70	9.55	9.86	9.64	9.45	10.41	10.09	14.27	10.33	10.24	10.66	10.25	10.43	10.44	10.79	10.67	10.62	10.80	10.09
Wo	34.26	40.34	41.18	41.13	40.87	41.24	41.35	38.45	40.71	29.14	39.49	39.66	38.77	39.65	39.08	41.09	40.67	39.78	40.78	40.27	39.47

Table 1. Cont

Sample	E3	E3	E3	E3	E3	E3	E3	E3	E3	E24	E24	E24	E24	E24	E24	E24	E24	E24	E24	E24	E24
No.	22	23	24	25	26	27	28	29	30	31	32	33	34	35	36	37	38	39	40	41	42
SiO_2	53.66	53.26	53.33	52.21	52.03	51.76	52.14	52.59	52.31	51.11	51.19	50.66	52.76	52.76	51.91	52.59	52.59	53.05	52.44	52.78	52.89
TiO_2	0.27	0.30	0.30	0.39	0.38	0.38	0.39	0.29	0.39	0.70	0.75	0.70	0.39	0.37	0.54	0.43	0.38	0.39	0.48	0.34	0.36
Al_2O_3	1.76	2.20	2.11	3.39	3.46	3.60	3.52	2.85	3.28	2.45	2.26	2.13	1.86	1.89	2.36	1.84	1.98	2.03	2.25	2.18	2.19
FeO	6.63	6.44	6.66	6.34	6.49	6.64	6.51	6.46	6.47	12.62	13.74	13.72	7.35	7.40	9.20	8.89	7.18	7.28	8.57	7.09	7.11
MnO	0.19	0.17	0.17	0.17	0.16	0.15	0.15	0.20	0.19	0.36	0.35	0.36	0.17	0.18	0.25	0.24	0.17	0.18	0.21	0.21	0.23
MgO	18.49	18.07	17.89	17.14	17.14	17.03	17.29	17.47	17.76	14.40	14.46	14.47	16.97	16.98	16.36	16.81	17.06	17.05	16.57	17.51	17.64
CaO	19.20	19.97	19.46	19.60	20.22	19.63	19.47	19.62	19.00	18.40	17.83	17.61	19.89	19.79	18.88	19.57	19.94	20.21	19.34	19.44	19.42
K_2O	0.00	0.00	0.00	0.00	0.01	0.00	0.00	0.00	0.00	0.00	0.00	0.00	0.01	0.00	0.00	0.00	0.01	0.00	0.00	0.01	0.00
Na_2O	0.18	0.19	0.20	0.24	0.26	0.23	0.23	0.24	0.24	0.28	0.25	0.26	0.22	0.19	0.22	0.24	0.15	0.19	0.25	0.20	0.20
Cr_2O_3	0.13	0.21	0.12	0.25	0.22	0.24	0.27	0.33	0.48	0.02	0.03	0.00	0.09	0.09	0.03	0.03	0.12	0.09	0.04	0.12	0.13
Total	100.5	100.81	100.25	99.74	100.38	99.67	99.96	100.05	100.12	100.33	100.87	99.91	99.71	99.65	99.74	100.64	99.58	100.46	100.15	99.87	100.17
Formula based on 6 oxygens																					
Si	1.947	1.928	1.943	1.913	1.894	1.899	1.906	1.921	1.907	1.908	1.907	1.904	1.942	1.944	1.921	1.926	1.938	1.938	1.929	1.935	1.933
Ti	0.007	0.008	0.008	0.011	0.010	0.011	0.011	0.008	0.011	0.020	0.021	0.020	0.011	0.010	0.015	0.012	0.011	0.011	0.013	0.009	0.010
Al (T)	0.053	0.072	0.057	0.087	0.106	0.101	0.094	0.079	0.093	0.092	0.093	0.094	0.058	0.056	0.079	0.074	0.062	0.062	0.071	0.065	0.067
Al (M1)	0.023	0.022	0.034	0.059	0.043	0.055	0.057	0.043	0.048	0.016	0.006	0.000	0.023	0.026	0.024	0.005	0.024	0.026	0.027	0.029	0.027
Fe^{3+} (T)	0.000	0.000	0.000	0.000	0.000	0.000	0.000	0.000	0.000	0.000	0.000	0.002	0.000	0.000	0.000	0.000	0.000	0.000	0.000	0.000	0.000
Fe^{3+} (M1)	0.025	0.041	0.017	0.016	0.055	0.035	0.025	0.028	0.027	0.056	0.062	0.075	0.026	0.020	0.040	0.062	0.024	0.025	0.035	0.029	0.031
Fe^{2+}	0.177	0.154	0.186	0.178	0.143	0.169	0.174	0.170	0.170	0.338	0.366	0.354	0.200	0.208	0.245	0.210	0.197	0.197	0.229	0.188	0.186
Mn	0.006	0.005	0.005	0.005	0.005	0.005	0.005	0.006	0.006	0.011	0.011	0.011	0.005	0.006	0.008	0.008	0.005	0.006	0.007	0.007	0.007
Mg	1.000	0.975	0.972	0.936	0.930	0.931	0.942	0.951	0.965	0.802	0.803	0.811	0.931	0.933	0.903	0.918	0.937	0.929	0.909	0.957	0.961
Ca	0.747	0.775	0.760	0.769	0.789	0.772	0.762	0.768	0.742	0.736	0.712	0.709	0.785	0.781	0.749	0.768	0.787	0.791	0.762	0.763	0.760
K	0.000	0.000	0.000	0.000	0.001	0.000	0.000	0.000	0.000	0.000	0.000	0.000	0.001	0.000	0.000	0.000	0.001	0.000	0.000	0.000	0.000
Na	0.013	0.014	0.014	0.017	0.019	0.016	0.016	0.017	0.017	0.021	0.018	0.019	0.016	0.014	0.016	0.017	0.011	0.013	0.018	0.014	0.014
Cr	0.004	0.006	0.004	0.007	0.006	0.007	0.008	0.009	0.014	0.001	0.001	0.000	0.003	0.003	0.001	0.001	0.003	0.003	0.001	0.003	0.004
Total	4.000	4.000	4.000	4.000	4.000	4.000	4.000	4.000	4.000	4.000	4.000	4.000	4.000	4.000	4.000	4.000	4.000	4.000	4.000	4.000	4.000
En	51.20	50.01	50.10	49.14	48.41	48.73	49.37	49.48	50.52	41.25	41.10	41.31	47.82	47.89	46.44	46.69	48.03	47.67	46.81	49.21	49.39
Fs	10.60	10.27	10.74	10.47	10.54	10.90	10.67	10.58	10.63	20.86	22.48	22.55	11.90	11.99	15.05	14.24	11.62	11.71	13.92	11.52	11.53
Wo	38.21	39.72	39.16	40.39	41.05	40.37	39.96	39.94	38.84	37.89	36.42	36.13	40.28	40.12	38.52	39.07	40.35	40.61	39.27	39.27	39.08

Table 1. Cont.

Sample	E24	E24	E24	E24	E24	E24	E24	E24	E24	E24	E24	E24	E24	E24	E24	E24	E24	E24	E24	E24	E24
No.	43	44	45	46	47	48	49	50	51	52	53	54	55	56	57	58	59	60	61	62	63
SiO_2	52.80	51.98	52.36	52.49	51.93	52.25	52.96	52.68	52.78	52.89	52.83	52.84	52.89	52.63	52.31	52.32	51.97	52.86	52.96	53.10	52.78
TiO_2	0.34	0.38	0.40	0.38	0.39	0.34	0.36	0.38	0.34	0.33	0.35	0.37	0.34	0.41	0.42	0.40	0.36	0.34	0.34	0.36	0.35
Al_2O_3	2.20	2.59	2.59	2.47	2.54	2.54	2.16	2.32	2.22	2.09	2.14	2.13	2.13	2.77	2.81	2.25	2.29	2.32	2.17	2.24	1.98
FeO	7.02	7.21	7.22	6.94	7.13	7.78	7.07	7.14	7.10	7.22	7.17	7.24	7.11	7.07	7.05	7.21	7.45	6.74	6.76	7.04	7.06
MnO	0.17	0.18	0.19	0.21	0.19	0.21	0.19	0.18	0.18	0.23	0.19	0.19	0.23	0.18	0.18	0.20	0.18	0.18	0.16	0.18	0.24
MgO	17.38	17.41	17.29	17.30	17.26	17.15	17.29	17.23	17.35	17.59	17.38	17.59	17.61	17.12	17.12	17.38	16.83	17.53	17.53	17.31	17.26
CaO	19.76	19.75	19.80	20.05	20.15	18.74	19.43	19.49	19.69	19.68	19.71	19.96	19.88	19.95	19.77	20.04	20.27	20.10	19.76	19.84	20.14
K_2O	0.00	0.00	0.01	0.00	0.00	0.00	0.00	0.01	0.01	0.00	0.00	0.00	0.00	0.00	0.01	0.00	0.00	0.00	0.00	0.00	0.01
Na_2O	0.21	0.20	0.20	0.19	0.22	0.21	0.20	0.20	0.23	0.26	0.18	0.22	0.21	0.25	0.22	0.23	0.26	0.23	0.21	0.18	0.19
Cr_2O_3	0.12	0.17	0.21	0.17	0.18	0.14	0.14	0.14	0.12	0.12	0.11	0.11	0.12	0.14	0.13	0.18	0.18	0.22	0.16	0.16	0.14
Total	100.00	99.88	100.28	100.20	99.99	99.36	99.80	99.76	100.01	100.41	100.07	100.64	100.52	100.52	100.02	100.21	99.80	100.52	100.05	100.41	100.15
Formula based on 6 oxygens																					
Si	1.933	1.905	1.913	1.918	1.902	1.929	1.944	1.935	1.933	1.928	1.934	1.922	1.926	1.918	1.916	1.912	1.911	1.924	1.937	1.938	1.932
Ti	0.009	0.011	0.011	0.010	0.011	0.010	0.010	0.010	0.009	0.009	0.010	0.010	0.009	0.011	0.011	0.011	0.010	0.009	0.009	0.010	0.010
Al (T)	0.067	0.095	0.087	0.082	0.098	0.071	0.056	0.065	0.067	0.072	0.066	0.078	0.074	0.082	0.084	0.088	0.089	0.076	0.063	0.062	0.068
Al(M1)	0.028	0.017	0.025	0.025	0.011	0.040	0.038	0.035	0.028	0.018	0.027	0.014	0.017	0.037	0.037	0.009	0.010	0.023	0.030	0.035	0.017
Fe^{3+}(T)	0.000	0.000	0.000	0.000	0.000	0.000	0.000	0.000	0.000	0.000	0.000	0.000	0.000	0.000	0.000	0.000	0.000	0.000	0.000	0.000	0.000
Fe^{3+} (M1)	0.031	0.066	0.048	0.045	0.076	0.023	0.008	0.019	0.033	0.051	0.029	0.056	0.049	0.036	0.037	0.068	0.072	0.045	0.025	0.015	0.042
Fe^{2+}	0.184	0.155	0.172	0.167	0.143	0.217	0.209	0.200	0.184	0.169	0.190	0.164	0.167	0.179	0.179	0.152	0.157	0.160	0.182	0.200	0.174
Mn	0.005	0.006	0.006	0.006	0.006	0.007	0.006	0.006	0.006	0.007	0.006	0.006	0.007	0.006	0.006	0.006	0.006	0.006	0.005	0.006	0.008
Mg	0.949	0.951	0.942	0.943	0.942	0.944	0.946	0.943	0.947	0.956	0.949	0.954	0.956	0.930	0.935	0.947	0.923	0.951	0.956	0.942	0.942
Ca	0.775	0.776	0.775	0.785	0.791	0.741	0.764	0.767	0.772	0.769	0.773	0.778	0.776	0.779	0.776	0.785	0.799	0.784	0.774	0.776	0.790
K	0.000	0.000	0.000	0.000	0.000	0.000	0.000	0.000	0.000	0.000	0.000	0.000	0.000	0.000	0.000	0.000	0.000	0.000	0.000	0.000	0.001
Na	0.015	0.014	0.014	0.014	0.015	0.015	0.014	0.014	0.016	0.018	0.013	0.015	0.015	0.018	0.016	0.017	0.019	0.016	0.015	0.012	0.014
Cr	0.003	0.005	0.006	0.005	0.005	0.004	0.004	0.004	0.004	0.003	0.003	0.003	0.003	0.004	0.004	0.005	0.005	0.006	0.005	0.005	0.004
Total	4.000	4.000	4.000	4.000	4.000	4.000	4.000	4.000	4.000	4.000	4.000	4.000	4.000	4.000	4.000	4.000	4.000	4.000	4.000	4.000	4.000
En	48.79	48.69	48.46	48.43	48.14	48.86	48.94	48.75	48.76	48.98	48.71	48.72	48.89	48.19	48.38	48.35	47.17	48.88	49.22	48.59	48.17
Fs	11.33	11.60	11.66	11.23	11.46	12.77	11.54	11.62	11.48	11.64	11.58	11.55	11.44	11.45	11.47	11.57	12.00	10.83	10.90	11.38	11.44
Wo	39.87	39.70	39.88	40.34	40.39	38.37	39.53	39.63	39.77	39.38	39.70	39.73	39.67	40.36	40.15	40.07	40.83	40.28	39.88	40.03	40.39

Table 1. Cont.

Sample	E24	E24	E24	E24	E24	E24	E24	E24	E24	E24	E24	E24	E24	E24	E24	E24	E24	E24	E24	E24	E24	E24
No.	64	65	66	67	68	69	70	71	72	73	74	75	76	77	78	79	80	81	82	83	84	85
SiO_2	52.78	53.00	52.89	52.96	52.93	52.82	52.90	52.82	52.74	52.82	51.38	52.10	52.34	52.14	52.81	52.48	52.69	52.57	52.57	52.60	51.29	51.18
TiO_2	0.36	0.38	0.40	0.41	0.38	0.40	0.43	0.45	0.44	0.45	0.55	0.52	0.50	0.46	0.48	0.46	0.48	0.45	0.45	0.45	0.70	0.72
Al_2O_3	1.98	2.15	1.87	2.05	1.95	2.03	2.03	2.02	2.00	2.00	2.04	1.77	1.64	1.87	1.64	1.61	1.64	1.68	1.85	1.86	2.11	2.07
FeO	7.14	7.13	7.33	7.13	7.35	7.80	7.97	8.32	8.47	8.83	13.48	13.92	12.70	12.40	11.68	11.75	11.60	11.57	11.99	12.20	13.71	13.66
MnO	0.15	0.21	0.20	0.17	0.19	0.19	0.20	0.22	0.21	0.23	0.38	0.36	0.35	0.34	0.30	0.32	0.31	0.32	0.34	0.34	0.35	0.39
MgO	17.21	16.96	16.94	16.91	17.08	16.88	16.77	16.78	16.71	16.74	15.38	16.17	16.45	16.60	16.86	16.81	16.91	16.86	16.84	16.79	14.34	14.27
CaO	20.04	20.06	20.14	20.53	20.56	20.36	20.14	20.07	19.72	19.29	16.58	15.85	16.25	16.73	16.91	17.07	17.31	17.15	16.43	16.28	17.89	17.69
K_2O	0.00	0.00	0.00	0.00	0.00	0.00	0.01	0.01	0.00	0.01	0.01	0.00	0.00	0.00	0.00	0.00	0.01	0.01	0.00	0.00	0.00	0.01
Na_2O	0.18	0.19	0.19	0.18	0.18	0.21	0.19	0.24	0.21	0.21	0.25	0.20	0.23	0.19	0.21	0.19	0.25	0.20	0.22	0.22	0.27	0.25
Cr_2O_3	0.14	0.16	0.04	0.10	0.11	0.06	0.05	0.03	0.02	0.00	0.00	0.00	0.02	0.00	0.00	0.00	0.00	0.00	0.02	0.02	0.02	0.00
Total	99.99	100.25	99.99	100.43	100.74	100.76	100.69	100.95	100.53	100.58	100.04	100.89	100.48	100.73	100.88	100.69	101.19	100.81	100.70	100.75	100.69	100.23
Formula based on 6 oxygens																						
Si	1.935	1.941	1.942	1.936	1.929	1.927	1.933	1.926	1.933	1.936	1.921	1.930	1.939	1.924	1.942	1.934	1.930	1.934	1.937	1.939	1.914	1.920
Ti	0.010	0.011	0.011	0.011	0.010	0.011	0.012	0.012	0.012	0.013	0.015	0.015	0.014	0.013	0.013	0.013	0.013	0.012	0.012	0.012	0.020	0.020
Al (T)	0.065	0.059	0.058	0.064	0.071	0.073	0.067	0.074	0.067	0.064	0.079	0.070	0.061	0.076	0.058	0.066	0.070	0.066	0.063	0.061	0.086	0.080
Al (M1)	0.021	0.033	0.023	0.024	0.013	0.014	0.021	0.013	0.019	0.022	0.011	0.007	0.011	0.006	0.013	0.004	0.001	0.007	0.018	0.019	0.007	0.011
Fe^{3+} (T)	0.000	0.000	0.000	0.000	0.000	0.000	0.000	0.000	0.000	0.000	0.000	0.000	0.000	0.000	0.000	0.000	0.000	0.000	0.000	0.000	0.000	0.000
Fe^{3+} (M1)	0.033	0.014	0.025	0.027	0.048	0.049	0.034	0.053	0.038	0.031	0.054	0.048	0.038	0.058	0.033	0.050	0.060	0.048	0.035	0.032	0.058	0.046
Fe^{2+}	0.186	0.205	0.201	0.191	0.176	0.189	0.210	0.201	0.221	0.239	0.367	0.383	0.355	0.325	0.326	0.312	0.296	0.307	0.335	0.344	0.370	0.383
Mn	0.005	0.007	0.006	0.005	0.006	0.006	0.006	0.007	0.006	0.007	0.012	0.011	0.011	0.011	0.009	0.010	0.010	0.010	0.011	0.011	0.011	0.012
Mg	0.941	0.926	0.927	0.922	0.928	0.918	0.914	0.912	0.913	0.915	0.857	0.893	0.909	0.913	0.924	0.924	0.924	0.925	0.925	0.923	0.798	0.798
Ca	0.787	0.787	0.792	0.804	0.803	0.796	0.789	0.784	0.774	0.758	0.664	0.629	0.645	0.662	0.666	0.674	0.679	0.676	0.649	0.643	0.715	0.711
K	0.000	0.000	0.000	0.000	0.000	0.000	0.001	0.000	0.000	0.000	0.000	0.000	0.000	0.000	0.000	0.000	0.000	0.000	0.000	0.000	0.000	0.000
Na	0.013	0.014	0.013	0.013	0.013	0.015	0.013	0.017	0.015	0.015	0.018	0.014	0.017	0.013	0.015	0.014	0.017	0.014	0.015	0.015	0.020	0.018
Cr	0.004	0.005	0.001	0.003	0.003	0.002	0.001	0.001	0.001	0.000	0.000	0.000	0.000	0.000	0.000	0.000	0.000	0.000	0.001	0.000	0.001	0.000
Total	4.000	4.000	4.000	4.000	4.000	4.000	4.000	4.000	4.000	4.000	4.000	4.000	4.000	4.000	4.000	4.000	4.000	4.000	4.000	4.000	4.000	4.000
En	48.20	47.78	47.53	47.29	47.33	46.89	46.80	46.61	46.74	46.91	43.85	45.46	46.40	46.40	47.18	46.88	46.93	47.02	47.35	47.26	40.87	40.93
Fs	11.46	11.61	11.85	11.46	11.72	12.46	12.80	13.32	13.62	14.25	22.17	22.52	20.65	19.98	18.81	18.90	18.55	18.61	19.45	19.81	22.49	22.61
Wo	40.34	40.61	40.61	41.26	40.95	40.65	40.40	40.07	39.64	38.85	33.98	32.02	32.94	33.61	34.01	34.22	34.52	34.37	33.20	32.93	36.64	36.46

Table 2. Composition and structural formula of plagioclase of Wadi Atalla El-Murr metabasalts, Central Eastern Desert, Egypt.

Sample	E3	E3	E3	E3	E3	E3	E3	E3	E24	E24	E24	E24	E24	E24	E24	E24	E24	E24
No.	1	2	3	4	5	6	7	8	9	10	11	12	13	14	15	16	17	18
SiO_2	66.22	51.89	52.21	49.81	55.26	64.79	65.06	59.55	59.77	58.23	67.38	58.41	58.55	58.82	69.45	68.25	69.56	68.98
TiO_2	0.00	0.03	0.05	0.06	0.06	0.00	0.00	0.02	0.01	0.03	0.01	0.01	0.04	0.01	0.00	0.00	0.00	0.00
Al_2O_3	22.32	29.20	28.95	30.23	26.96	22.28	23.08	25.21	25.10	25.74	21.43	25.60	25.81	25.52	20.56	21.45	20.47	20.76
FeO	0.17	0.95	1.00	0.95	0.93	0.47	0.39	0.98	0.58	0.65	0.28	0.65	0.58	0.61	0.42	0.31	0.49	0.34
CaO	2.29	13.48	13.24	14.45	10.67	2.62	2.15	5.94	7.35	8.16	1.33	8.29	8.23	8.04	0.11	0.81	0.13	0.30
Na_2O	9.31	3.43	3.73	2.90	4.89	9.51	9.00	7.11	6.82	6.47	9.26	6.42	6.35	6.62	9.89	9.28	8.94	9.47
K_2O	0.14	0.13	0.12	0.11	0.13	0.08	0.61	0.83	0.22	0.19	0.13	0.21	0.20	0.20	0.10	0.10	0.07	0.09
Total	100.45	99.11	99.31	98.51	98.90	99.76	100.28	99.63	99.85	99.47	99.81	99.59	99.76	99.83	100.53	100.20	99.67	99.94
Formula based on 32 oxygens																		
Si	11.541	9.538	9.580	9.250	10.087	11.427	11.398	10.688	10.683	10.487	11.759	10.508	10.504	10.548	11.989	11.831	12.060	11.964
Ti	0.000	0.005	0.007	0.008	0.008	0.000	0.000	0.002	0.001	0.003	0.001	0.002	0.005	0.001	0.000	0.000	0.000	0.000
Al	4.585	6.325	6.260	6.616	5.800	4.631	4.765	5.332	5.287	5.463	4.407	5.428	5.457	5.393	4.183	4.382	4.182	4.243
Fe^{2+}	0.024	0.146	0.154	0.148	0.142	0.070	0.057	0.147	0.087	0.098	0.041	0.097	0.086	0.092	0.061	0.045	0.072	0.050
Ca	0.428	2.655	2.603	2.875	2.087	0.495	0.404	1.142	1.407	1.574	0.248	1.598	1.582	1.545	0.021	0.150	0.025	0.056
Na	3.146	1.222	1.327	1.044	1.731	3.252	3.057	2.474	2.363	2.259	3.133	2.239	2.209	2.302	3.310	3.119	3.005	3.184
K	0.031	0.031	0.028	0.027	0.030	0.019	0.136	0.189	0.050	0.043	0.028	0.048	0.047	0.046	0.022	0.023	0.016	0.019
Total	19.75	19.92	19.96	19.97	19.88	19.89	19.82	19.97	19.88	19.93	19.62	19.92	19.89	19.93	19.58	19.55	19.36	19.52
An	11.86	67.94	65.77	72.86	54.24	13.15	11.22	30.02	36.84	40.61	7.29	41.13	41.22	39.68	0.61	4.56	0.82	1.71
Ab	87.28	31.28	33.53	26.46	44.98	86.36	85.01	65.02	61.86	58.27	91.89	57.64	57.56	59.12	98.74	94.75	98.64	97.71
Or	0.85	0.78	0.70	0.68	0.78	0.50	3.77	4.96	1.31	1.11	0.82	1.23	1.22	1.19	0.64	0.69	0.54	0.58

Table 2. Cont.

Sample No.	E24 19	E24 20	E24 21	E24 22	E24 23	E24 24	E24 25	E24 26	E24 27	E24 28	E24 29	E24 30	E24 31	E24 32	E24 33	E24 34	E24 35	E24 36
SiO_2	54.79	56.30	69.49	69.46	69.74	66.92	57.82	57.11	57.32	57.31	57.29	64.49	67.33	68.39	58.05	66.49	56.95	67.09
TiO_2	0.05	0.01	0.00	0.00	0.01	0.01	0.00	0.01	0.02	0.01	0.02	0.00	0.00	0.00	0.02	0.01	0.01	0.01
Al_2O_3	27.67	26.99	20.61	20.80	20.45	21.94	26.22	26.59	26.59	26.43	26.40	23.13	20.81	20.89	25.96	21.59	26.67	21.25
FeO	0.67	0.53	0.28	0.32	0.32	0.28	0.51	0.49	0.45	0.38	0.48	0.36	0.15	0.21	0.68	0.41	0.65	0.34
CaO	10.93	9.57	0.12	0.11	0.34	1.97	8.42	8.92	8.79	7.83	8.67	2.80	0.51	0.24	8.77	2.15	9.37	1.82
Na_2O	5.00	5.63	9.49	9.67	8.85	6.83	6.29	6.04	6.03	6.00	6.10	8.31	9.63	9.02	6.06	8.87	5.79	8.88
K_2O	0.13	0.11	0.10	0.07	0.08	0.15	0.18	0.17	0.17	0.16	0.18	0.39	0.06	0.05	0.18	0.29	0.18	0.26
Total	99.24	99.14	100.10	100.43	99.78	98.10	99.44	99.33	99.37	98.12	99.14	99.48	98.50	98.80	99.73	99.81	99.62	99.65
Formula based on 32 oxygens																		
Si	9.975	10.205	12.017	11.983	12.070	11.786	10.415	10.315	10.338	10.421	10.358	11.372	11.871	11.964	10.437	11.653	10.274	11.747
Ti	0.007	0.001	0.000	0.000	0.001	0.001	0.000	0.001	0.003	0.001	0.003	0.000	0.000	0.000	0.003	0.001	0.002	0.001
Al	5.937	5.765	4.200	4.229	4.171	4.554	5.566	5.660	5.652	5.664	5.625	4.807	4.324	4.307	5.501	4.459	5.670	4.385
Fe^{2+}	0.102	0.080	0.041	0.046	0.046	0.041	0.076	0.074	0.067	0.058	0.073	0.053	0.022	0.030	0.103	0.060	0.099	0.050
Ca	2.132	1.858	0.023	0.021	0.063	0.372	1.625	1.726	1.698	1.525	1.679	0.529	0.097	0.045	1.689	0.404	1.811	0.341
Na	1.765	1.978	3.182	3.234	2.969	2.332	2.197	2.115	2.108	2.115	2.138	2.841	3.292	3.059	2.112	3.014	2.025	3.014
K	0.030	0.026	0.023	0.016	0.018	0.034	0.042	0.039	0.040	0.036	0.042	0.089	0.014	0.011	0.042	0.066	0.041	0.059
Total	19.95	19.91	19.49	19.53	19.34	19.12	19.92	19.93	19.91	19.82	19.92	19.69	19.62	19.42	19.89	19.66	19.92	19.60
An	54.30	48.12	0.70	0.63	2.06	13.58	42.05	44.49	44.16	41.49	43.51	15.29	2.84	1.45	43.95	11.59	46.71	10.00
Ab	44.95	51.22	98.60	98.89	97.35	85.18	56.85	54.51	54.82	57.53	55.40	82.14	96.75	98.21	54.95	86.53	52.23	88.28
Or	0.76	0.66	0.71	0.48	0.60	1.24	1.09	1.00	1.03	0.99	1.08	2.56	0.40	0.34	1.10	1.88	1.06	1.72

Table 3. Composition of Wadi Atalla El-Murr metabasalts, Central Eastern Desert

Sample	E3A	E3B	E8C	E7B2	E15A	E15B	E18A	E18B	E24A	E24B	E25B	E28B1	E28B2
SiO_2	49.38	49.12	50.33	51.91	47.08	47.27	49.72	44.60	48.53	48.64	48.15	48.11	47.71
TiO_2	1.15	1.15	1.11	1.08	1.06	1.11	1.06	1.19	1.25	1.27	0.88	0.88	0.89
Al_2O_3	13.57	13.83	13.76	14.16	15.32	14.51	13.44	13.15	14.33	14.49	15.03	14.75	14.42
Fe_2O_3	12.21	12.14	11.09	10.59	12.08	11.97	10.16	11.15	12.61	12.73	10.82	10.19	10.31
MnO	0.20	0.20	0.19	0.20	0.19	0.20	0.19	0.20	0.20	0.20	0.17	0.16	0.16
MgO	7.12	7.07	6.87	6.38	7.74	8.13	7.23	7.60	7.11	7.14	9.26	9.30	9.59
CaO	10.48	10.64	11.19	9.94	9.85	12.41	9.14	10.87	10.07	10.14	9.89	10.95	10.69
Na_2O	2.62	2.44	2.41	3.57	2.59	1.87	3.22	2.67	2.83	2.50	2.48	2.64	2.59
K_2O	0.45	0.49	0.45	0.26	0.16	0.15	0.94	0.63	0.42	0.45	0.48	0.39	0.39
P_2O_5	0.11	0.11	0.11	0.11	0.10	0.11	0.11	0.12	0.12	0.12	0.08	0.08	0.08
LOI	2.16	2.36	1.87	1.56	2.78	2.33	4.00	7.08	2.03	2.00	2.69	2.40	2.47
Total	99.49	99.56	99.40	99.78	99.01	100.12	99.23	99.31	99.53	99.71	100.01	99.93	99.39
Sc	42.17	44.26	39.68	45.11	45.16	42.44	39.92	44.98	43.74	44.32	41.70	40.58	41.68
V	295.05	308.72	286.91	312.98	279.85	297.17	271.31	285.56	302.59	301.54	245.20	240.11	237.68
Cr	89.02	95.05	78.74	82.57	286.28	312.40	106.06	125.21	100.13	94.33	382.24	417.99	429.84
Co	50.65	51.01	45.92	48.81	49.98	51.48	42.54	44.55	46.02	43.02	46.15	46.55	46.88
Ni	49.89	52.52	41.69	58.01	78.24	89.02	44.07	47.26	55.63	51.81	106.66	114.10	112.09
Cu	109.74	104.56	107.74	106.50	154.88	65.96	6.36	5.09	68.64	72.63	95.73	107.63	104.99
Zn	72.40	74.01	68.48	72.97	66.28	55.21	58.86	64.76	62.80	56.96	49.51	42.84	41.31
Ga	13.44	14.58	13.52	14.12	11.98	14.43	11.68	12.87	14.90	14.41	12.58	11.02	10.76
Rb	8.67	9.48	9.17	4.27	2.19	2.13	22.34	13.86	8.96	9.56	10.93	7.07	7.79
Sr	206.07	205.43	189.59	248.04	172.73	216.11	200.92	197.05	172.45	167.49	210.16	156.79	153.26
Y	21.52	21.43	19.05	21.78	17.08	19.21	19.98	21.77	23.56	23.01	16.10	15.82	15.45
Zr	64.16	63.44	59.55	59.72	55.56	56.59	62.42	70.60	74.56	73.31	45.09	43.87	42.24
Nb	3.14	3.38	3.24	3.02	2.84	2.83	3.01	3.40	3.19	3.58	2.23	2.27	2.33
Ba	91.90	91.01	76.49	74.57	51.21	38.41	178.81	141.77	73.90	76.59	102.61	125.24	110.75
La	4.65	4.68	4.53	4.53	3.73	3.63	4.27	5.35	4.94	4.67	2.83	3.23	3.18
Ce	11.69	12.43	12.04	11.43	9.72	9.56	11.19	13.13	12.82	12.43	7.99	8.24	8.44
Pr	1.77	1.83	1.85	1.65	1.44	1.42	1.69	2.01	1.94	1.91	1.13	1.26	1.27
Nd	9.71	9.40	8.99	8.43	7.37	7.50	7.97	9.55	9.86	9.67	5.94	6.50	6.54
Sm	2.79	2.71	2.45	2.59	2.14	2.70	2.57	3.33	3.21	2.95	2.05	2.21	2.43
Eu	1.00	0.98	0.94	1.02	0.93	0.93	0.56	0.88	0.87	0.86	0.43	0.80	0.81
Gd	3.50	3.39	3.18	3.38	3.24	3.05	3.49	3.61	4.05	3.97	2.73	2.89	2.92
Tb	0.59	0.60	0.59	0.59	0.52	0.52	0.55	0.64	0.69	0.62	0.46	0.44	0.41
Dy	4.21	4.14	3.48	3.70	2.82	3.53	3.34	4.33	4.09	4.12	2.60	2.69	2.86
Ho	0.79	0.86	0.73	0.82	0.73	0.70	0.72	0.89	0.90	0.80	0.59	0.67	0.61
Er	2.35	2.54	2.27	2.58	1.92	1.90	2.03	2.56	2.56	2.64	1.86	1.83	1.64
Tm	0.36	0.33	0.31	0.32	0.32	0.32	0.27	0.36	0.42	0.32	0.25	0.23	0.26
Yb	2.27	2.46	1.91	2.49	1.97	2.19	2.07	2.49	2.29	2.27	1.88	2.03	1.53
Lu	0.34	0.31	0.28	0.33	0.29	0.30	0.29	0.33	0.32	0.38	0.21	0.23	0.27
Hf	1.60	1.82	1.76	1.77	1.56	1.36	1.63	2.03	2.08	2.02	1.22	1.02	1.22
Ta	0.26	0.27	0.26	0.26	n.d.	0.17	0.18	0.24	0.24	0.23	0.18	0.15	0.15
Pb	1.06	1.05	1.07	1.63	0.55	0.82	0.86	1.01	0.29	0.25	0.21	0.29	0.33
Th	0.50	0.52	0.57	0.50	0.32	0.30	0.50	0.58	0.51	0.60	0.24	0.24	0.30
U	0.15	0.16	0.13	0.10	n.d.	0.04	0.19	0.21	0.17	0.17	0.10	0.04	0.07

n.d: not detected.

The MORB-normalized patterns of the basalts (Fig. 5A) show variable enrichment in LILE, variable depletion in Zr, Hf, Sm, Ti, Y and Yb, and small negative Nb anomaly, reflecting subduction component in their magma source. Ta and Ce range from slightly enriched to slightly depleted relative to N-MORB. The chondrite-normalized REE patterns of the basalts (Fig. 5B) display slight enrichment in LREE relative to HREE (La/Yb_n = 1.08-1.70). Eu anomalies range from slightly positive to markedly negative (Eu/Eu* = 1.08-0.56). The slightly positive Eu anomalies suggest some plagioclase accumulation, while the strongly negative anomalies reflect significant plagioclase fractionation.

DISCUSSION

Tectonic setting: back-arc or nascent island arc?

The volcanic rocks of the study area were mapped as island arc volcanics (Bakhit, 1994; Basta et al., 1996). The chemical characteristics of the pyroxenes of Wadi Atalla El-Murr basalts resemble those of pyroxenes of ocean-floor and island arc basalts and are similar to those of pyroxenes of basalts erupted along modern back-arcs such as Lau Basin (Fig. 3C and D). Moreover, the MORB-normalized spider diagrams of the basalts (Fig. 5A) display small Nb trough and LILE enrichment, implying subduction component in the mantle source of the parental magma produced Wadi Atalla El-

Murr basalts. However, plotting the analyzed basalts on different tectonomagmatic discrimination diagrams (Fig. 6A-D) suggests that they were erupted on ocean floor rather than in island arc setting.

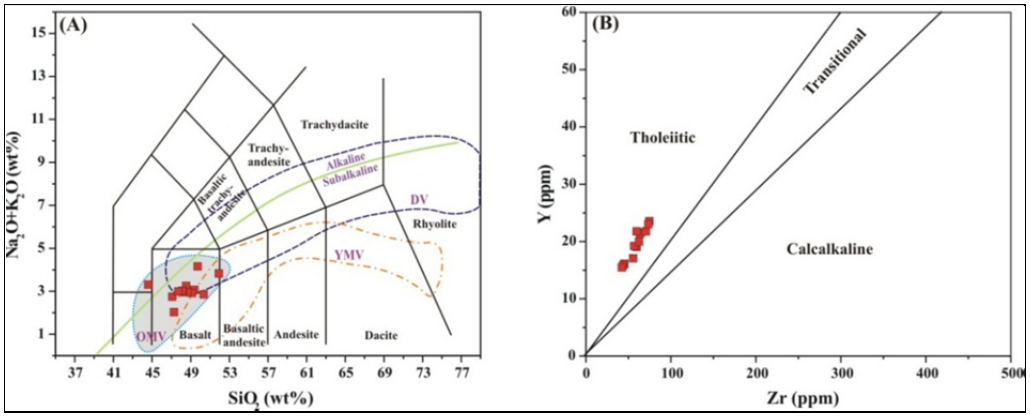

Fig. 4. Classification and magma type of Wadi Atalla El-Murr mafic volcanic rocks. (A) SiO_2 versus Na_2O+K_2O diagram (after Le Bas et al., 1986), (B) Zr-Y diagram (after Barrett and MacLean, 1994). The fields of Older metavolcanics (OMV), Younger metavolcanics (YMV) and Dokhan volcanics (DV) are adopted from Eliwa et al. (2006) and references therein. The dividing line between subalkaline and alkaline fields after Irvine and Baragar (1971).

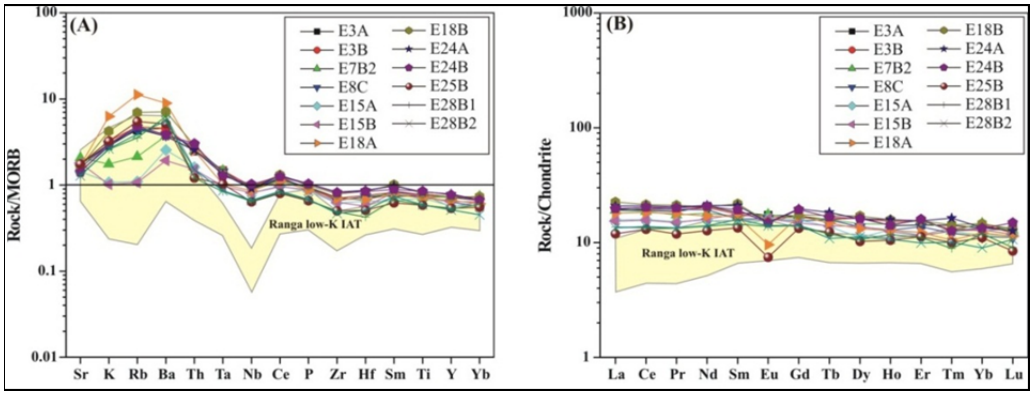

Fig. 5. (A) MORB-normalized spider diagrams and (B) Chondrite-normalized REE patterns for Wadi Atalla El-Murr metabasalts. MORB normalization values after Pearce (1983); Chondrite normalization values after Sun and McDonough (1989). Data of Wadi Ranga IAT after Maurice et al. (2012).

Tholeiitic basalts like those of Wadi Atalla El-Murr can be generated along spreading centers or in intra-oceanic island arc setting (Wilson, 1989). To evaluate the possibility of generation of Wadi Atalla El-Murr Neoproterozoic basalts in nascent island arc, the geochemical features of these basalts have been compared with those of Wadi Ranga Neoproterozoic basalts which were extruded in nascent intra-oceanic island arc setting (Maurice et al., 2012). Although they plot close to those of Wadi Atalla El-Murr basalts, the pyroxenes of Wadi Ranga and Wadi Atalla El-Murr tholeiites do not overlap (Fig. 3). On the different tectonomagmatic discrimination diagrams, it is evident that Wadi Ranga IAT and Wadi Atalla El-Murr basalts occupy island arc and MORB or BABB fields (Fig. 6), respectively. Moreover, the spider diagrams of these tholeiitic basalts are different, where the patterns of Wadi Ranga IAT display stronger depletion in HFSE and very marked Nb trough compared with those of the basalts of Wadi Atalla El-Murr (Fig. 5A). The Wadi Atalla El-Murr basalts have REE abundances higher than those of Wadi Ranga IAT (Fig. 5B), and their chondrite-normalized REE patterns display slight LREE-enrichment (La/Yb_n = 1.08-1.70) while those of Wadi Ranga ITA are characterized mostly by LREE-depletion (La/Yb_n = 0.49-1.03). In short, the geochemical features of Wadi Ranga IAT and Wadi Atalla El-Murr basalt are not alike, ruling out the extrusion of Wadi Atalla El-Murr basalts in nascent intra-oceanic island arc.

The mixed MORB/IAT geochemical and mineral chemical characteristics of the Wadi Atalla El-Murr basalts resemble those of basalts generated in modern back-arc environments such as Scotia Sea, Lau Basin and Mariana Trough (e.g. Tarney et al., 1981; Saunders and Tarney, 1984; Pearce et al., 1995; 2005; Fretzdorff et al., 2002; Keller et al., 2008), and are best explained by generation of the parental melts of these basalts along spreading center located close to subduction zone, i.e. along Neoproterozoic back-arc spreading center. Additionally, plotting the analyzed samples on the Ti-V

(Shervais, 1982) and La-Y-Nb (Cabanis and Lecolle, 1989) diagrams (Fig. 6C and D), supports back-arc environment for the generation of Wadi Atalla El-Murr basalts.

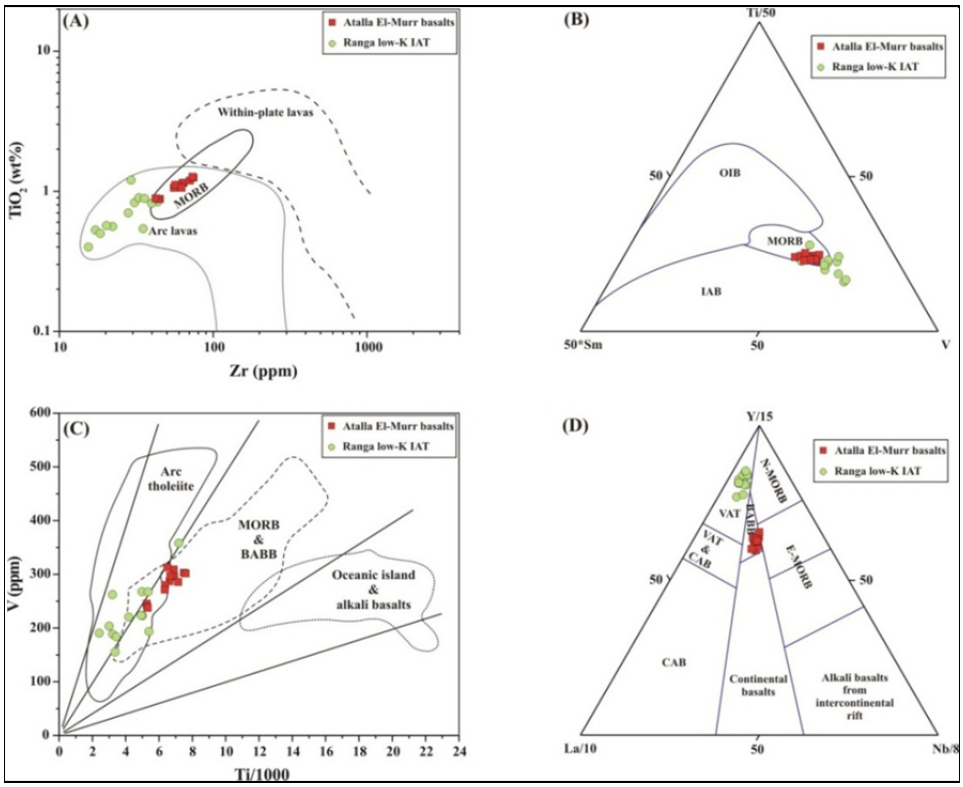

Fig. 6. Tectonic setting of Wadi Atalla El-Murr metabasalts. (A) Zr-TiO_2 diagram (after Pearce, 1982), (B) Sm-Ti-V diagram (after Vermeesch, 2006), (C) Ti-V diagram (after Shervais, 1982), (D) La-Y-Nb diagram (after Cabanis and Lecolle, 1989). Data of Wadi Ranga IAT after Maurice et al. (2012).

Petrogenesis

The depletion of most HFSE in Wadi Atalla El-Murr basalts compared with N-MORB (Fig. 5A) indicates that the mantle source of the parental magmas of these basalts was more depleted than N-MORB mantle source. Additionally, Most of the trace elements abundances of the Wadi Atalla El-Murr basalts are lower than those of the Neoproterozoic N-MORB of Gerf ophiolite (Fig. 7), supporting mantle source more depleted than N-MORB mantle source. The Nb and Zr-Hf troughs characteristic for the trace elements patterns of Wadi Atalla El-Murr basalts compared with the Neoproterozoic N-MORB of Gerf ophiolite (Fig. 7), indicate SSZ mantle source for these basalts (Pearce, 2014). On the Th/Yb vs Nb/Yb diagram (Pearce, 2014), the Neoproterozoic Wadi Atalla El-Murr basalts plot close to or above the MORB-OIB array (Fig. 8A), suggesting subduction component in the mantle source of their parental magma. This is supported by LILE-enrichment relative to MORB (Fig. 5A) and the slight enrichment in LREE relative to HREE (La/Yb_n = 1.08-1.70) of Wadi Atalla El-Murr basalts (Fig. 5B). Although the analyzed samples of Wadi Atalla El-Murr plot within the mantle array on the La/Yb vs Nb/Yb diagram (Fig. 8B), their La/Yb values are higher than N-MORB value implying contribution of small amount of LREE through subduction component. The enrichment of Wadi Atalla El-Murr metabasalts in fluid mobile elements compared with MORB (Fig. 5A) suggest subducted fluid component in their mantle source. On the other hand, the higher Th abundances in these metabasalts compared with N-MORB (Figs. 7 and 8A) can be attributed to subducted sediments (Plank, 2005; Tian et al., 2011) during deep subduction (Pearce and Stern, 2006). However, the subduction component was not significant as indicated by slight LREE-enrichment on their REE patterns (Fig. 5B). The variable Mg# (52.7-64.8) of Wadi Atalla El-Murr basalts together with Eu anomaly values ranging from slightly positive to markedly negative (Eu/Eu* = 1.08-0.56) indicate that some of these basalts do not represent primitive basaltic melts and their compositions have been modified by fractionation before eruption.

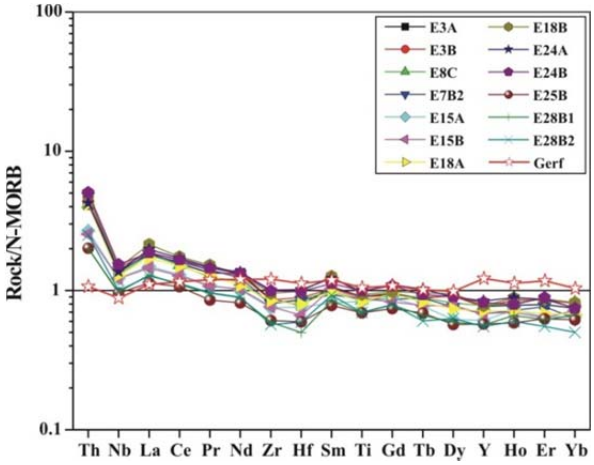

Fig. 7. N-MORB-normalized trace elements of Wadi Atalla El-Murr and the average of Neoproterozoic N-MORB of Gerf ophiolite. Normalization values after Sun and McDonough (1989).

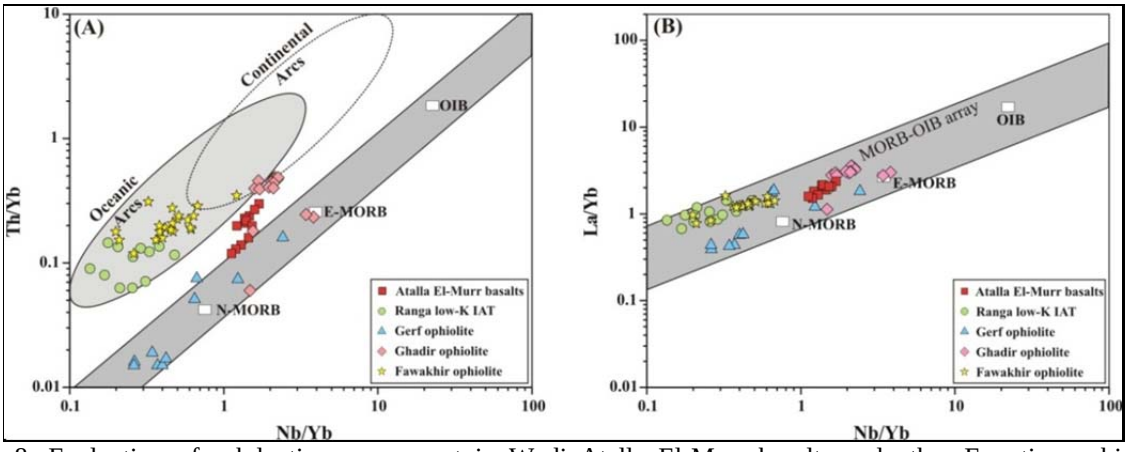

Fig. 8: Evaluation of subduction component in Wadi Atalla El-Murr basalts and other Egyptian ophiolite metavolcanics, the Neoproterozoic Wadi Ranga IAT is shown for comparison. (A) Th/Yb vs Nb/Yb diagram (after Pearce, 2014), (B) La/Yb vs Nb/Yb diagram, the MORB-OIB array after Green (2006). Data sources: Wadi Atalla El-Murr ophiolite metavolcanics (present study), Gerf ophiolite (Zimmer et al., 1995); Wadi Ghadir ophiolite (Basta et al., 2011); Fawakhir ophiolite (Abd El-Rahman et al., 2009b); Wadi Ranga IAT (Maurice et al., 2012).

Back-arc basin maturity

Although they are formed along spreading centers, back-arc basin basalts (BABB) and MORB may differ in geochemical features (Fryer et al., 1981; Tarney et al., 1981). Studies of volcanic rocks of modern back-arcs such as Lau Basin, Mariana Trough and East Scotia Sea showed that the composition of basalts varied spatially along the different segments of back-arc ridge from MORB-like to arc-like (Tarney et al., 1981; Pearce et al., 1995, 2005; Keller et al., 2008). Such variations have been attributed to the maturity of adjacent subduction zone, the proximity of spreading centers to subducted slab, the maturity or evolution of back-arc basin and the differences in the degree of mantle depletion (Tarney et al., 1981; Saunders and Tarney, 1984; Pearce et al., 1995; 2005; Fretzdorff et al., 2002; Pearce and Stern, 2006; Keller et al., 2008; Tian et al., 2011). Back-arc basins formed during the earliest stages of subduction erupt volcanics with MORB-like composition, whereas basalts formed during the early stages of back-arc spreading in mature subduction zone have arc-like composition (Tarney et al., 1981; Saunders and Tarney, 1984; Keller et al., 2008). Back-arc spreading centers present close to arc erupt basalts with arc signature, while those located far from trench produce MORB-like volcanics (e.g. Pearce et al., 1995). The subduction signature in back-arc magmas gradually decreases with increasing the distance from the arc. Moreover, the composition of the subduction component of basalts of Lau Basin varies with the proximity of the spreading center to the arc (Pearce et al., 1995).

The N-MORB-normalized trace elements patterns of Wadi Atalla El-Murr basalts (Fig. 7) display Nb troughs characteristic for SSZ ridge settings, and small Zr-Hf troughs characteristic for BABB erupted along spreading center adjacent to arcs (Pearce, 2014). On the Th/Yb vs Nb/Yb diagram (Pearce, 2014), the Neoproterozoic back-arc basalts of Wadi Atalla El-Murr plot close to or above the MORB-OIB array (Fig. 8A), suggesting subduction component in their mantle source. Plotting the

analyzed basalts on the Th_N-Nb_N diagram of Saccani (2015) shows that most of the samples lie along the boundary between the fields of immature and mature intra-oceanic back-arcs (Fig. 9A), suggesting eruption of these volcanics during immature-mature transition stage or during the earliest mature stage of Neoproterozoic intra-oceanic back-arc basin. This conclusion is supported by the fact that some of the analyzed samples plot in the overlap area between the arc and MORB/BABB fields on the Ti-V diagram (Fig. 6C) of Shervais (1982).

Implication for the composition, settings and classification of ANS ophiolites

The ophiolite metavolcanics of Egypt have compositions ranging from basalts to basaltic andesites with occasional andesites (e.g. El-Sharkawy and El-Bayoumi, 1979; Basta, 1983; Abd Rl-Rahman et al., 2009a & b; Basta et al., 2011). To evaluate the compositional variations of the ophiolite metavolcanics of the Eastern Desert, the composition of samples from the ophiolites of Gerf (Zimmer et al., 1995), Wadi Ghadir (Basta et al., 2011) and Fawakhir (Abd Rl-Rahman et al., 2009b) has been plotted on the Th_N-Nb_N diagram of Saccani (2015). This diagram (Fig. 9B) showed that the metavolcanic rocks of Egyptian ophiolites comprise MORB and BABB compositions, and the MORB composition varies from depleted through normal to enriched. Such variation in the MORB composition implies Neoproterozoic mantle heterogeneity (Khedr and Arai, 2016).

The ophiolites are classified into subduction-unrelated and subduction-related types (Dilek and Furnes, 2014). The former comprise continental margin, mid-ocean ridge and plume-types, while the latter include fore/back-arc suprasubduction zone and volcanic arc types. Based on the geochemical affinities of the ophiolite metavolcanic rocks, Abd El-Rahman et al. (2012) classified the ophiolites of the Central Eastern Desert of Egypt into fore-arc and back-arc types. They suggested that the fore-arc and back-arc ophiolites are preserved in the western and eastern parts of the Central Eastern Desert, respectively. Recently, El Bahariya (2018) divided the ophiolites of the Central Eastern Desert of Egypt into MORB or BABB and SSZ types, although BABB ophiolite is considered sub-type of SSZ ophiolites (Dilek and Furnes, 2014). He proposed that these ophiolites are temporally and spatially unrelated and their setting has been changed with time from MORB to SSZ.

Figures 8A and 9A showed that the tectonic settings of the metavolcanics of the famous ophiolites of the Eastern Desert comprise subduction-unrelated (Gerf) and subduction-related (present study, Wadi Ghadir, Fawakhir) types. In the subduction-related types, the magnitude of subduction input to the mantle source of the Neoproterozoic ophiolite metavolcanics of the Eastern Desert varied from small (present study) to significant (Fawakhir), implying generation at variable distances from adjacent arcs during different stages of evolutions of Neoproterozoic SSZ systems.

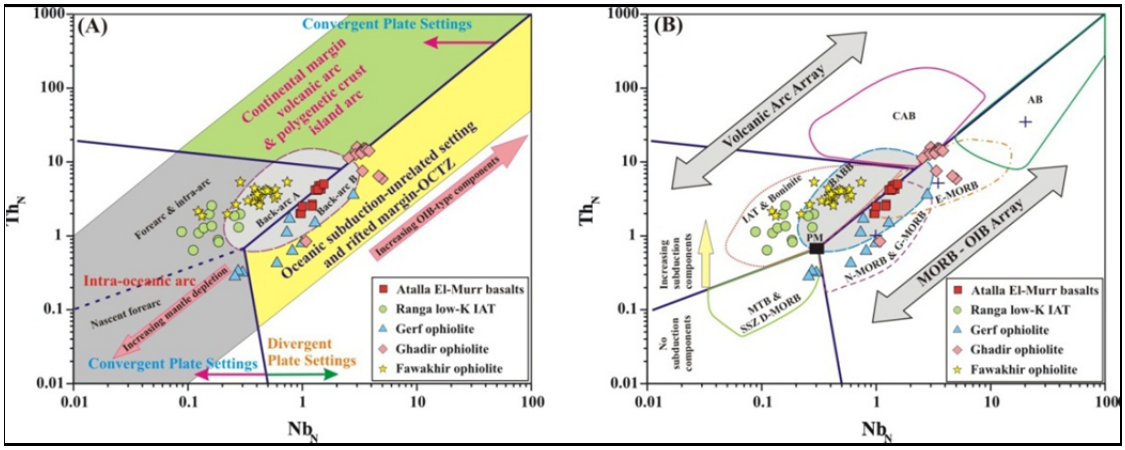

Fig. 9: Th_N versus Nb_N diagram (after Saccani, 2015) to evaluate (A) the tectonic settings and (B) the compositions of Egyptian ophiolite metavolcanics. Th and Nb are normalized to N-MORB values of Sun and McDonough (1989). Back-arc A, BABB with subduction component; Back-arc B, BABB with no subduction input. Data sources as in Fig. 8.

CONCLUSIONS

1- The Wadi Atalla El-Murr metabasalts are composed of pyroxene and plagioclase with texture varying from very fine-grained through vitrophyre to porphyritic which reflects variable degrees of cooling from quenching to slower cooling rate.

2- The pyroxenes are represented by augites while the plagioclases range in composition from labradorite (An = ~73%) to albite (An = 0.61%), reflecting seafloor hydrothermal alteration and metamorphism.
3- The analyzed pyroxenes are similar to those crystallize from subalkaline magmas and have chemical characteristics overlapping those of the pyroxenes of island arc and ocean-floor basalts.
4- The metabasalts of Wadi Atalla El-Murr have low K_2O contents (<1 wt%) and tholeiitic affinity, similar to oceanic tholeiites produced by partial melting of depleted mantle sources.
5- The Wadi Atalla El-Murr basalts generally occupy the MORB or BABB field on conventional tectonomagmatic discrimination diagrams. However, the REE patterns of the metabasalts display slight enrichment in LREE relative to HREE (La/Yb_n = 1.08-1.70) and the MORB-normalized spider diagrams show variable LILE enrichment, variable depletion in most HFSE and small negative Nb anomaly, reflecting subduction component in a depleted mantle source.
6- The mixed MORB/IAT geochemical characteristics of the Wadi Atalla El-Murr basalts resemble those of basalts generated in modern back-arc environments affected by minor subduction component.
7- The small arc geochemical signature in the Wadi Atalla El-Murr basalts is consistent with eruption in Neoproterozoic mature back-arc basin and rules out the possibility of formation of these tholeiites in Neoproterozoic nascent intra-oceanic island arc environment.
8- The compositional characteristics of Wadi Atalla El-Murr BABB are consistent with eruption along spreading center at intermediate distance from the adjacent arc during immature-mature transition stage or during the earliest mature stage of Neoproterozoic intra-oceanic back-arc basin.
9- The metavolcanic rocks of Egyptian ophiolites comprise MORB and BABB compositions, and the MORB composition varies from depleted through normal to enriched.
10- The ophiolites of the Eastern Desert comprise subduction-unrelated (Gerf) and subduction-related (present study, Wadi Ghadir, Fawakhir) types. Variable magnitude of subduction signature in the metavolcanics of the Egyptian SSZ ophiolites reflects generation at variable stages of evolution of Neoproterozoic SSZ systems.

ACKNOWLEDGEMENTS

The author expresses his gratitude to Prof. Dr. Bottros R. Bakhit, Beni-Suef University, for the electron microprobe and geochemical analyses conducted at ETH-Zürich, Switzerland. Prof. Dr. Fawzy Basta, Cairo University, is acknowledged for fruitful discussions and reading an earlier version of the manuscript. The author whishes to thank Prof. Dr. Paul Asimow, Caltech, USA, for reading part of the manuscript, and Prof. Dr. Baher El-Kaliouby and Dr. Nahla Abd El-Ghaffar for editorial handling.

REFERENCES

Abdel-Rahman, A. M. (1996): Pan-African volcanism: petrology and geochemistry of the Dokhan Volcanic suite in the northern Nubian Shield. Geol. Mag., 133, 17-31.

Abd El-Rahman, Y., Polat, A., Dilek, Y., Fryer, B., El-Sharkawy, M. and Sakran, S. (2009a): Geochemistry and tectonic evolution of the Neoproterozoic Wadi Ghadir Ophiolite, Eastern Desert, Egypt. Lithos, 113 (1-2), 158-178.

Abd El-Rahman, Y., Polat, A., Dilek, Y., Fryer, B., El-Sharkawy, M. and Sakran, S. (2009b): Geochemistry and tectonic evolution of the Neoproterozoic incipient arc-forearc crust in the Fawakhir area, Central Eastern Desert of Egypt. Precamb. Res., 175, 116-134.

Abd El-Rahman, Y., Polat, A., Dilek, Y., Kusky, T.M., El-Sharkawi, M. and Said, A. (2012): Cryogenian ophiolite tectonics and metallogeny of the Central Eastern Desert of Egypt. Inter. Geol. Rev., 54 (16), 1870-1884.

Abdel-Karim, A. M., Ali, S., El-Awady, A., Elwan, W., Khedr, M. and Akihiro, T. (2019): Mineral and bulk-rock chemistry of Shadli bimodal metavolcanics from Eastern Desert of Egypt: Implication for tectonomagmatic setting and Neoproterozoic continental growth in the Arabian-Nubian Shield. Lithos, 338-339, 204-217.

Ali, K. A., Stern, R. J., Manton, W. I., Kimura, J.-I. and Khamees, H. A. (2009): Geochemistry, Nd isotopes and U-Pb SHRIMP zircon dating of Neoproterozoic volcanic rocks from the Central Eastern Desert of Egypt: New insights into the ~750 Ma crust-forming event. Precamb. Res., 171, 1-22.

Bakhit, B. R. (1994): Gold mineralization in some occurrences of the Eastern Desert, Egypt. M.Sc Thesis, Cairo Univ., 214p.

Barrett, T. J., MacLean, W. H., (1994): Chemostratigraphy and hydrothermal alteration in exploration for VHMS deposits in greenstone and younger volcanic rocks. In: Lentz, D. R. (Ed.), Alteration and Alteration Processes Associated with Ore-Forming Systems. Geological Association of Canada, Short Course Notes, vol. 11, 433–467.

Basta, E. Z., Kotb, H. and Awadalla, M. F. (1980): Petrochemical and geochemical characteristics of the Dokhan Formation at the type locality, Jabal Dokhan, Eastern Desert, Egypt. Inst. Appl. Geol. Jeddah Bull., 3, 121-140.

Basta, F. F., (1983): Geology and geochemistry of the ophiolitic mélange and other rock units in the area around and west of Gabal Ghadir, Eastern Desert, Egypt. Ph.D. thesis, Cairo University, 137p.

Basta, F. F., Maurice, A. E., Bakhit, B. R., Ali, K. A. and Manton, W. I. (2011): Neoproterozoic Contaminated MORB of Wadi Ghadir Ophiolite, NE Africa: Geochemical and Nd and Sr isotopic Constraints. J. Afr. Earth Sci., 59, 227-242.

Basta, F. F., Maurice, A. E., Bakhit, B. R., Azer, M. K. and El-Sobky, A. F. (2017): Intrusive rocks of the Wadi Hamad area, North Eastern Desert, Egypt: change of magma composition with maturity of Neoproterozoic continental island arc and the role of collisional plutonism in the differentiation of arc crust. Lithos, 288-289, 248-263.

Basta, F. F., Takla, M. A. and Bakhit, B. R. (1996): Gold mineralization of Atalla and Semna areas, Eastern Desert, Egypt. Third Inter. Conf. Geol. Arab World, 63-86.

Beccaluva, L., Macciotta, G., Piccardo, G. B. and Zeda, O. (1989): Clinopyroxene of ophiolite basalts as petrogenetic indicator. Chem. Geol., 77, 165-182.

Cabanis, B. and Lecolle, M., (1989): Le diagramme La/10-Y/15-Nb/8: un outil pour la discrimination des séries volcaniques et la mise en évidence des procésses de mélange et/ou de contamination crustale. C. R. Acad. Sci., 2, 2023-2029.

Dilek, Y. and Furnes, H. (2014): Ophiolites and their origins. Elements 10, 93-100.

El Bahariya, G. A. (2018): Classification of the Neoproterozoic ophiolites of the Central Eastern Desert, Egypt based on field geological characteristics and mode of occurrence. Arab. J. Geosci., 11, 313.

Eliwa, H. A., Kimura, J.-I. and Itaya, T. (2006): Late Neoproterozoic Dokhan Volcanics, North Eastern Desert, Egypt: Geochemistry and petrogenesis. Precamb. Res., 151, 31-52.

El-Sayed, M. M., Furnes, H. and Mohamed, F. H. (1999): Geochemical constraints on the tectonomagmatic evolution of the late Precambrian Fawakhir ophiolite, Central Eastern Desert, Egypt. J. Afr. Earth Sci., 29 (3), 515-533.

El-Sharkawy, M. A. and El-Bayoumi, R. (1979): The ophiolites of Wadi Ghadir area, Eastern Desert, Egypt. Ann. Geol. Surv. Egypt, 9, 125-135.

Essawy, M. A. and Abu Zeid, K. M. (1972): Atalla felsite intrusion and its neighbouring rhyolitic flows and tuffs, Eastern Desert. Ann. Geol. Surv. Egypt, 2, 271-280.

Fretzdorff, S., Livermore, R. A., Devey, C. W., Leat, P. T. and Stoffers, P. (2002): Petrogenesis of the back-arc east Scotia Ridge, South Atlantic Ocean. J. Petrol., 43, 1435-1467.

Fryer, B., Sinton, J. M. and Philpotts, J. A. (1981): Basaltic glasses from the Mariana Trough. DSDP initial reports, 60, 601-609.

Ghoneim, M.F. (1973): Geology of the area around Bir El-Kubbania, Eastern Desert, Egypt. M. Sc. thesis, Tanta Univ., Egypt.

Green, N. L. (2006): Influence of slab thermal structure on basalt source regions and melting conditions: REE and HFSE constraints on from the Garibaldi volcanic belt, northern Cascadia subduction system. Lithos, 87, 23-49.

Gribble, R. F., Stern, R. J., Newman, S., Bloomer, S. H. and O'Hearn, T. (1998): Chemical and isotopic composition of lavas from the northern Mariana Trough: Implications for magmagenesis in back-arc basins. J. Petrol., 39, 125-154.

Hirahara, Y., Kimura, J.-I., Senda, R., Miyazaki, T., Kawabata, H., Takahashi, T., Chang, Q., Vaglarov, B. S., Sato, T. and Kodaira, S. (2015): Geochemical variations in Japan Sea back-arc basin basalts formed by high- temperature adiabatic melting of mantle metasomatized by sediment subduction components, Geochem. Geophys. Geosyst., 16, 1324 - 1347, doi:10.1002/2015GC005720.

Hawkins, J. W. and Allan, J. F. (1994): Petrologic evolution of the Lau Basin, Sites 834-839. Proc. Ocean Drill. Program Sci. Results, 135, 427-470.

Irvine, T.N. and Baragar, W.R.A., (1971): A guide to the chemical classification of the common volcanic rocks. Can. J. Earth Sci., 8, 523-548.

Keller, N. S., Arculus, R. J., Hermann, J. and Richards, S. (2008): Submarine back-arc lava with arc signature: Fonualei Spreading Center, northeast Lau Basin, Tonga. J. Geophys. Res., 113, B08S07, doi:10.1029/2007JB005451.

Khedr, M.Z. and Arai, S. (2016): Petrology of a Neoproterozoic Alaskan-type complex from the Eastern Desert of Egypt: implications for mantle heterogeneity. Lithos, 263, 15-32.

Le Bas, M. J., Le Maitre, R. W., Streckeisen, A. and Zanettin, B. (1986): A chemical classification of volcanic rocks based on the total alkali-silica diagram. J. Petrol., 27, 745-750.

Leterrier, J., Maury, R. C., Thonon, P., Girard, D. and Marchal, M. (1982): Clinopyroxene composition as a method of identification of the magmatic affinities of paleo-volcanic series. Earth Planet. Sci. Lett., 59, 139-154.

Maurice, A. E., Bakhit, B. R., Basta, F. F, Asimow, P. D., Wälle, M, Azer, M. K. and El-Sobky, A. F. (2018): The last subduction-related volcanism in the northern tip of the Arabian-Nubian Shield: A Neoproterozoic arc preceding the terminal collision of East and West Gondwana. Precamb. Res., 310, 256-277.

Maurice, A. E., Basta, F. F. and Khiamy, A. A. (2012): Neoproterozoic nascent island arc volcanism from the Nubian Shield of Egypt: magma genesis and generation of continental crust in intra-oceanic arcs. Lithos, 132-133, 1-20.

Moghazi, A. M. (2003): Geochemistry and petrogenesis of a high-K calc-alkaline Dokhan Volcanic suite, South Safaga area, Egypt: the role of late Neoproterozoic crustal extension. Precamb. Res., 125, 161-178.

Morimoto, N., Fabries, J., Ferguson, A. K., Ginzburg, I. V., Ross, M., Seifert, F. A., Zussman, J., Aoki, K. and Gottardi, G. (1988): Nomenclature of pyroxenes. Mineral. Mag., 52, 535-550.

Nisbet, F. G. and Pearce, J. A. (1977): Clinopyroxene composition in mafic lavas from different tectonic settings. Contrib. Mineral. Petrol., 63, 149-160.

Pearce, J. A. (1982): Trace element characteristics of lavas from destructive plate boundaries. In: Thorpe, R. S. (Ed.), Andesites. Wiley, Chichester, 525-548.

Pearce, J. A. (1983): Role of the subcontinental lithosphere in magma genesis at active continental margins. In: Hawkesworth, C.I. and Norry, M.J. (eds.), Continental basalts and mantle xenoliths. Shiva, Nantwich, 230-249.

Pearce, J. A. (2014): Immobile element fingerprinting of ophiolites. Elements 10, 101-108.

Pearce, J. A., Stern, R. J., Bloomer, S. and Fryer, P. (2005): Geochemical mapping of the Mariana arc-basin system: implications for the nature and distribution of subduction components. Geochem. Geophys. Geosyst., 6, Q07006. doi:10.1029/2004GC000895.

Pearce, J. A., Ernewein, M., Bloomer, S. H., Parson, L. M., Murton, B. J. and Johnson, L. E. (1995): Geochemistry of Lau Basin volcanic rocks: influence of ridge segmentation and arc proximity, In Smellie, J. L. (Ed.), Volcanism Associated with Extension at Consuming Plate Margins. Geol. Soc. Spec. Publ., 81, 53-75.

Pearce, J. A. and Stern, R. J. (2006): Origin of back-arc basin magmas: trace element and isotope perspectives. Geophysical Monograph Series, 166, 63-86.

Plank, T. (2005): Constraints from thorium/lanthanum on sediment recycling at subduction zones and the evolution of continents. J. Petrol., 46, 921-944.

Polat, A., Hofmann, A.W. and Rosing, M.T. (2002): Boninite-like volcanic rocks in the 3.7-3.8 Ga Isua greenstone belt, West Greenland: Geochemical evidence for intra-oceanic subduction zone processes in the Early Earth. Chem. Geol., 184, 231-254.

Ressetar, R. and Monard, J. R. (1983): Chemical composition and tectonic setting of the Dokhan Volcanic formation, Eastern Desert, Egypt. J. Afr. Earth Sci., 1, 103-112.

Saccani, E. (2015): A new method of discriminating different types of post-Archean ophiolitic basalts and their tectonic significance using Th-Nb and Ce-Dy-Yb systematics. Geosci. Front., 6, 481-501.

Saunders, A. D. and Tarney, J. (1984): Geochemical characteristics of basaltic volcanism within back-arc basins. Geol. Soc. Lond. Spec. Publ., 17, 59-76.

Shervais, J. W. (1982): Ti-V plots and the petrogenesis of modern and ophiolitic lavas. Earth Planet. Sci. Lett., 59, 101-118.

Shinjo, R., Chung, S.-L., Kato, Y. and Kimura, M. (1999): Geochemical and Sr-Nd isotopic characteristics of volcanic rocks from Okinawa Trough and RyuKyu Arc: implications for the evolution of a young, intracontinental back arc basin. J. Geophys. Res., 104 (B5), 10591-10608.

Sinton, J. M., Ford, L. L., Chappell, B. and McCulloch, M. T. (2003): Magma genesis and mantle heterogeneity in the Manus Back-Arc Basin, Papua New Guinea. J. Petrol., 44, 159-195.

Stern, R. J. (1981): Petrogenesis and tectonic setting of Late Precambrian ensimatic volcanic rocks, central Eastern Desert of Egypt. Precamb. Res., 16, 195-230.

Sun, S. S. and McDonough, W. F. (1989): Chemical and isotope systematics of oceanic basalts, implications for mantle composition and processes. In Saunders, A.D. and Norry, M.J. (Eds.), Magmatism in ocean basins. Geol. Soc. Lond. Spec. Publ., 42, 313-345.

Taman, Z. (1996): Geology and mineralization of Wadi Atalla area, Eastern Desert, Egypt. M.Sc thesis, Ain Shams Univ., 120 p.

Tarney, J., Saunders, A. D., Mattey, D. P. and Wood, D. A. (1981): Geochemical aspects of back-arc spreading in the Scotia Sea and western Pacific. Phil. Trans. R. Soc. Lond., A300, 263-285.

Tian, L., Castillo, P. R., Hilton, D. R., Hawkins, J. W., Hanan, B. B. and Pietruszka, A. J. (2011): Major and trace element and Sr-Nd isotope signatures of the northern Lau Basin lavas: Implications for the composition and dynamics of the back-arc basin mantle, J. Geophys. Res., 116, B11201, doi:10.1029/2011JB008791.

Vallier, T. L., Jenner, G. A., Frey, F. A., Gill, G. B., Davis, A. S., Volpe, A. M., Hawkins, J. W., Morris, J. D., Cawood, P. A., Morton, J. L., Scholl, D. W., Rautenschlein, M., White, W. M., Williams, R.W., Stevenson, A. J. and White, L. D. (1991): Subalkaline andesite from Valu Fa Ridge, a back-arc spreading center in southern Lau Basin: petrogenesis, comparative chemistry and tectonic implications. Chem. Geol., 91, 227-256.

Vermeesch, P. (2006): Tectonic discrimination diagrams revisited. Tectonic discrimination diagrams revisited, Geochem. Geophys. Geosyst., 7, Q06017, doi:10.1029/2005GC001092.

Wassef, B., Kamel, O. A., Armanious, L. K. and Sabet, A. H. (1973): Report on the results of the prospecting work for gold in El Sid-Semna area in 1970/1971. Geol. Surv. Egypt, internal report no. 23/1973.

Wilson, M. (1989): Igneous petrogenesis - A global tectonic approach. Unwin Hyman Ltd., 466p.

Zimmer, M., Kröner, A., Jochum, K. P., Reischmann, T. and Todt, W. (1995): The Gabal Gerf complex: A Precambrian N-MORB ophiolite in the Nubian Shield, NE Africa. Chem. Geol., 123, 29-51.

بترولوجية وجيوكيميائية البازلت المتحول بوادى عطاالله المُر، الصحراء الشرقية، مصر: بركنه فى حوض خلف قوس ناضج نيوبروتيروزوى

أيمن البدرى موريس

قسم الجيولوجيا – كلية العلوم – جامعة حلوان

الخلاصة

تشتمل الصخور البركانية المافية بوادى عطاالله المر، الصحراء الشرقية، مصر، على صخور بازلت بورفيرى وغير بورفيرى مكونة من معادن البيروكسين والبلاجيوكلاز التى تغيرت بدرجات متفاوته. تتكون الحبيبات الكبيرة فى صخور البازلت البورفيرى أساساً من معدن الأوجيت الذى يتواجد فى شكل حبيبات منفصلة أو فى شكل تجمعات مكونةً نسيج جلوميروبورفيرى. يُظهر البلاجيوكلاز مدى واسع من التغير فى التركيب من اللابرادوريت إلى الألبيت مما يعكس تغير وتحول حرمائى على قاع البحر. يؤكد تركيب معدن الأوجيت تبلور من ماجما تحت قاعدية، ويتراكب مع السمات الكيميائية للبيروكسين الموجود فى بازلت الجزر القوسية وبازلت قاع المحيط. أظهرت التحاليل الكيميائية لصخور البازلت أن تلك الصخور تتميز بمحتوى قليل من أكسيد البوتاسيم (أقل من ١%) وذات طبيعة ثولييتية . تُظهر نماذج العناصر الأرضية النادرة المعايرة للكوندريت لصخور البازلت غنىً طفيف فى العناصر الأرضية النادرة الخفيفة بالنسبة للعناصر الأرضية النادرة الثقيلة (La/Ybn = 1.08–1.70) ، بينما تُظهر النماذج العنكبوتية المعايرة للمورب تنوع فى الغنى فى العناصر ذات الأيونات الكبيرة المحبة للصخور، وتنوع فى الإستنضاب فى العناصر ذات المجال العالى القوة، وشذوذ سالب صغير فى عنصر النيوبيوم مما يعكس نشأة من وشاح مُطعّم بمكون إندساس . ومع ذلك ، تختلف السمات الكيميائية لذلك البازلت الثولييتى عن تلك التى للصخور الثوليتية النيوبروتيروزوية التى تكونت فى قوس جزيرى غير ناضج كما أن عينات البازلت تقع فى مجالات المورب أو البازلت المتكون فى حوض خلف قوس على الأشكال التى تستخدم فى تمييز البيئات التكتونوماجماتية المختلفة . تشبه السمات الكيميائية الهجين بين المورب وثولييت الجزر القوسية لبازلت عطاالله المر تلك التى للبازلت الذى يتكون فى أحواض خلف القوس الحديثة والتى تأثرت بالقليل من إضافات إندساس، مما يعنى تكون أثناء المرحلة الناضجة الأبكر لحوض خلف قوس نيوبروتيروزوى. تظهر البيانات الحالية والمنشورة للصخور البركانية المتحولة التى تتبع صخور الأوفيوليت المصرية أن تلك الصخور تشتمل على تركيبات بازلت حوض خلف القوس والمورب . إن معظم صخور بركانيات الأوفيوليت المتحولة بمصر قد تكونت فى بيئات تكتونية مرتبطة بالإندساس من وشاح أُغنى بمكون الإندساس بدرجات متفاوتة من زهيدة إلى كبيرة ، مما يعكس نشأة أثناء مراحل مختلفة خلال تطور أنظمة فوق نطاق إندساس نيوبروتيروزوية .

بترولوجية وجيوكيميائية سربنتين أوفيوليتى بمنطقة أم عش، الصحراء الشرقية، مصر: وشاح نيوبروتيروزوى من بيئة فوق نطاق الإندساس متحول

أيمن البدرى موريس

قسم الجيولوجيا – كلية العلوم – جامعة حلوان

الخلاصة

يشتمل السربنتين الأوفيوليتى النيوبروتيروزوى لمنطقة أم عش بوسط الصحراء الشرقية المصرية على أنواع كتلية ومرققه والتى تتكون أساساً من معدن الأنتيجوريت مع قليل من معدن الكروم سبينيل. تتمثل معادن الكربونات بالماجنيزيت الذى يتواجد فى شكل تجمعات أو عُريقات. تكون حبيبات الكروم سبينيل متنطقه دائماً، من لُب طازج أو بقايا طازجه محاطة بحواف من الفريت كروميت والماجنيتيت الحاوى على الكروم. يتميز الكروم سبينيل الأوّلى بمحتوى قليل جداً من أكسيد التيتانيوم (أقل من ٠.٠٢٥ %) وكذلك قيم قليلة (٠.٠١٠ –٠.٠١٦) لنسبة أكسيد الألومنيوم إلى أكسيد السيليكون مما يوضح أن صخور السربنتين تمثل وشاح متبقى تعرّض لدرجه عالية من الأنصهار الجزئى. ويتشابه محتوى الكروم سبينيل الأوّلى من أكسيد الألومنيوم (١٦–٢٥%) وأكسيد التيتانيوم (٠.٠٠٧ % فى المتوسط) مع تلك التى لصخور البريدوتيت المتكونه فى بيئة فوق نطاق الإندساس وبيئة تلال وسط المحيط. ولكن الطبيعة شديدة الإستنضاب لسربنتين منطقة أم عش وكذلك ال #Cr و #Mg للكروم سبينيل الأوّلى تتشابه مع تلك التى لصخور البريدوتيت المتكون أمام القوس لبيئة فوق نطاق الإندساس.

وأظهرت قطاعات للتركيب الكيميائى للنطاقات المختلفة للكروم سبينيل المتنطق أن تركيزات أكاسيد الكروم والمغنسيوم والألومنيوم قد إنخفضت فجأة بينما إزدادت بسرعة تركيزات أكسيد الحديد وكذلك #Fe من الكروم سبينيل الطازج إلى الفريت كروميت إلى الماجنيتيت الحاوى على الكروم، كما أن التغير فى تركيزات تلك الأكاسيد كان متدرجاً داخل النطاق الواحد من نطاقات السبينيل المتحول. وعلى الجانب الأخر فأن تركيزات أكاسيد النيكل والمنجنيز تتغير بشكل غير منتظم من اللُب إلى الحافة .

تؤكد سيادة معدن الأنتيجوريت فى صخور السربنتين ووجود حواف من السبينيل المتحول حول الكروم سبينيل الأوّلى أن صخور سربنتين أم عش قد تعرضت إلى تحول فى سحنة الأمفيبوليت السفلى فى ظروف بيئة مؤكسدة.